Maximizing Local Access to Therapeutic Deliveries in Glioblastoma: Evaluating the utility and mechanisms of potential adverse events for minimally invasive diagnostic two novel therapeutic techniques for brain tumors

Yukitaka Steve Kani Kani

Dissertation submitted to the faculty of the Virginia Polytechnic Institute and State University in partial fulfillment of the requirements for the degree of

Doctor of Philosophy
In
Biomedical and Veterinary Sciences

John H. Rossmeisl, Chair
John Robertson
Thomas Cecere
Scott Verbridge

September 19, 2022
Blacksburg, VA

Keywords: brain biopsy, glioma, glutamate, high-frequency electroporation, convection enhanced delivery

Maximizing Local Access to Therapeutic Deliveries in Glioblastoma: Evaluating the utility and mechanisms of potential adverse events for minimally invasive diagnostic two novel therapeutic techniques for brain tumors

Yukitaka Steve Kani Kani

ACADEMIC ABSTRACT

Glioblastoma (GBM) is the most common adult malignant glioma (MG) variant, and the median survival of persons with GBM is about 2 years, even with aggressive treatments. Dogs and humans are the only species in which brain tumors commonly develop spontaneously, with an estimated post-mortem frequency of primary brain tumors approximating 2% in both species. Gliomas represent about 35% of all canine primary brain tumors, with high-grade oligodendroglioma and astrocytoma phenotypes accounting for about 70% of all canine gliomas. Canine gliomas are also treated using surgical, radiotherapeutic, and chemotherapeutic regimens similar to those used in humans. The efficacy of these therapies in dogs with MG is also poor, with median survival times ranging from 3-8 months, which closely mirrors the dismal prognosis associated with human GBM. Thus, treatment of MG represents a current and critically unmet need in both human and veterinary medicine.

In this work, we investigate minimally invasive methods to access the brain for the purposes of ultimately improving the diagnosis and treatment of malignant brain tumors. **Chapter 1** reviews the current clinical challenges associated with the treatment of GBM, highlights the value of using the spontaneous canine glioma model in translational brain tumor studies, and introduces High-Frequency Irreversible Electroporation (H-FIRE) and Convection Enhanced Delivery (CED), which are two novel treatment platforms for GBM being developed in our lab. In **Chapter 2**, we demonstrate that definitive diagnosis of brain tumors, a critical first step in patient management, can be safely and accurately performed in dogs with naturally occurring brain tumors using a stereotactic brain biopsy procedure. **Chapter 3** evaluates the *in vivo* safety and biocompatibility of fiberoptic microneedle devices, a major technical component of our convection-enhanced

thermotherapy catheter system (CETCS), chronically implanted in the rodent brain. The CETCS is a novel technology being developed and used in our laboratory to improve the delivery of drugs to brain tumors using CED. This study provides regulatory data fundamental to the commercialization of the CETCS device for brain tumor treatment by illustrating that the device did not cause clinically significant neurological complications and resulted in mild pathologic changes in brain tissue, similar to other types of devices designed and approved for use in the brain.

In **Chapters 4 and 5** we explore possible bystander effects of H-FIRE on glutamate metabolism in the brain. H-FIRE has been shown to be able to both ablate brain tumors as well as disrupt the blood-brain barrier (BBB). As these therapeutic effects of H-FIRE are dependent on applying electrical fields to the tissue that either reversibly permeabilize the cell membrane, allowing treated cells to survive, or permanently disrupt the structure of the cell membrane, causing cell death, we hypothesized that altering the membrane permeability with HFIRE would increase the extracellular glutamate concentrations and contribute to excitotoxic brain tissue damage. **Chapters 4** used *in vitro* brain cell culture systems and *in vivo* experiments in normal and glioma-bearing rat brains to determine if glutamate release in the brain occurs as a bystander effect following H-FIRE treatment, identify concentrations of glutamate necessary to induce death of cells or BBB disruption, and characterize glutamatergic gene expression in response to H-FIRE treatment. **Chapter 5** describes the use of magnetic resonance spectroscopic and spatial transcriptomic methods to further quantify the *in vivo* effects of H-FIRE treatment on glutamate release and metabolism in dogs with spontaneous brain tumors. The *in vitro* results indicated that the magnitude of glutamate release following H-FIRE is insufficient to induce cytotoxicity in normal or neoplastic brain cell lines, and also did not increase the permeability of the BBB. In our *in vivo* model systems, we documented significant, transient post-H-FIRE increases in glutamate to concentrations previously associated with excitotoxicty, with upregulation of the expression of genes involved with ionotropic and metabotropic glutamatergic receptor signaling. A contemporaneous upregulation of genes associated with glutamate uptake and recycling were also noted, indicating an adaptive, protective response to the glutamate release.

Our work summarily demonstrates that the diagnosis and potential treatment of malignant brain tumors can be achieved through the use of minimally invasive techniques that provide local access to brain tissue. While complications will always be possible anytime the brain is manipulated surgically, and further investigations are required to characterize the spectrum and mechanisms of adverse events that can occur following CETCS CED and H-FIRE treatment, our results support the continued development of these novel therapeutic platforms for the treatment of GBM.

Maximizing Local Access to Therapeutic Deliveries in Glioblastoma: Evaluating the utility and mechanisms of potential adverse events for minimally invasive diagnostic and two novel therapeutic techniques for brain tumors

Yukitaka Steve Kani Kani

GENERAL AUDIENCE ABSTRACT

Glioblastoma (GBM) is the most common adult malignant brain tumor, and the average survival of persons with GBM is about 2 years, even with aggressive treatments. Dogs and humans share common characteristics of the presentation of brain tumors, and the available treatment options are similar to those used in humans, such as surgical, radiotherapeutic, and chemotherapeutic regimens. The efficacy of these therapies in dogs with malignant brain tumors is also poor, with survival times ranging from 3-8 months, which closely mirrors the prognosis associated with human GBM. Thus, treatment of malignant gliomas represents a current and critically unmet need in both human and veterinary medicine.

This work describes how minimally invasive surgical procedures that involve placement of small diameter needles, electrodes, or catheters into the brain tissue for the purposes of obtaining a piece of tumor for diagnosis or delivering energy or drugs to kill tumor cells can be used effectively for the management of patients with brain cancer, and evaluates the types and possible causes of complications associated with of these procedures. We first demonstrate that stereotactic brain biopsy, a procedure that has been previously rarely described in dogs, is a safe and accurate method for the diagnosis of brain tumors in this species. Next, we demonstrate that a specialized type of catheter, termed the convection-enhanced thermotherapy catheter system (CETCS) that is used in our lab for use for direct drug delivery into brain tumors, can be implanted into the brain of rats for long periods of time without causing serious clinical complications or damage to the brain tissue, findings which support its use for repeated treatments of brain cancer. The final chapters investigate how an innovative treatment for brain cancer called high-frequency irreversible electroporation (H-FIRE) that uses electrical energy to kill cells may cause alterations in the brain microenvironment characterized by an excess of the neurotransmitter glutamate

that could predispose patients to developing undesirable complications of treatment such as brain tissue death outside of the intended treatment area, damage to the blood-brain barrier, or seizures. While we did demonstrate that H-FIRE treatment does transiently increase the glutamate concentrations in the brain of rats and dogs with brain tumors, we also showed that the brain's natural systems for deactivating and recycling glutamate were activated following treatment, which may mitigate the clinical appearance of any glutamate-associated side effects.

The knowledge that generated in this work has contributed to defining the clinical utility and safety profiles of these novel techniques, which will facilitate their more widespread use to treat dogs with brain cancer, and supports the further development and commercialization of CETCS and H-FIRE for future use in humans with GBM.

DEDICATION

This work is dedicated to my beloved parents Kiyotaka and Hiroko, who gave me unconditional support during my years in the PhD program. Their trust in me was always an extra boost to continue until the end.

To Ximе, my partner. She was one of the first person who believe in my potential to do the PhD, and had the strength to wait for me all these years in Chile.

To Gaviota, Coto who I left in my parent's home during the program, and passed away. I will use all this knowledge to continue helping to improve the small animal health.

ACKNOWLEDGEMENTS

First, I would like to sincerely thank my great advisor Dr. John Rossmeisl. He was always supportive and enthusiast during the whole doctorate program, always attentive to my needs, present to discuss ideas and results. Without his support everything would have been very different. Thank you very much to be the best advisor and mentor that I ever had. He was a great example to follow for my academic development.

Second, I have to acknowledge my committee members: Dr. John Robertson, Dr. Tom Cecere and Dr. Scott Verbridge. In all the meetings we had, they were always very interested in the work done, and their comments were essential for my constant improvement.

My "Veterinary and Comparative Neuro-oncology Laboratory" members: Jonathan Hinckley, Brittanie Partridge, Josefa García, and the Biomedical Engineering lab members Melvin Lorenzo, Sabrina Campello, Nastaran Alinezhadbalalami. They were important people who contribute actively in all the experiments we did, and beloved partners in my doctorate program. They undoubtedly made my PhD program the best.

Finally, I would like recognize the Institute for Critical Technology and Science as well as the Brain Tumor center of excellence at Wake Forest Cancer Center. The Large Animal Models Core, Central Nervous System Tissue Biorepository, and portions of this work were supported by grants from the National Institutes of Health (P30CA012197, P01CA207206, R01CA139099, and R01CA213423).

TABLE OF CONTENTS

LIST OF TABLES

LIST OF FIGURES

CHAPTER 1. BACKGROUND AND SIGNIFICANCE

Malignancies of the central nervous system (CNS) are the third leading cause of cancer-related deaths in adolescents and adults 15 - 34 years old, and the leading cause of cancer death in children [1]. Glioblastoma (GBM) is the most common adult malignant primary brain tumor, and the median survival of patients with GBM is about 2 years, even using a combination of treatments, such as radiation and chemotherapy [2]. There are several factors that are responsible for the difficulty in treating GBM: complete surgical removal is almost impossible because the margins of the tumor are not well defined and invade healthy brain tissue[3]; the presence of the blood-brain barrier (BBB) is another important factor because it limits the chemotherapy drug delivery, providing both physical and biochemical barriers [4]; and a final factor is tumor heterogeneity. One chemotherapeutic agent that is frequently used in the conventional treatment is temozolomide because it is capable of passing through the BBB, but the expression of methylguanine methyl transferase (MGMT) by glioma cells counteracting the mechanism of action makes them resistant to the drug [5]. Therefore, GBM's aggressively proliferative, heterogeneous and chemotherapy resistant nature highly compromises the available therapeutic options, leading to recurrence and death. Clearly, more effective treatment for GBM is urgently needed.

In the dog, primary intracranial neoplasia represents ~2–5% of all cancers. The most common types of tumors are represented by meningiomas (~50%), gliomas (~35%), and choroid plexus tumors (~7%) [6, 7]. Brain tumors in dogs occur at any age and in any breed. However, most primary brain tumors occur in middle-aged to older dogs, with the majority of cases described being > 5 years of age [7, 8]. Specifically for gliomas, some epidemiologic data associated are a median age at diagnosis of 8 years, a male predilection (incidence ratio of 1.53 for males/females), and predominant lesion location within the fronto-olfactory, temporal, and parietal lobes of the brain [9].

Different imaging techniques are frequently used for the diagnosis of primary intracranial tumors as a first approach. Among the most used are cross-sectional diagnostic imaging techniques, such as computed tomography (CT) and magnetic resonance imaging (MRI)[10]. MRI is the preferred modality for the assessment of animals with intracranial disease because it provides valuable

information about tumor structure, margination, vascularization, hydration, as well as peritumoral edema and inflammation that allow us to approach the diagnosis [11]. Currently, tissue biopsies are the gold-standard technique for GBM diagnosis. However, this technique can present risks to the patients, such as possible brain swelling within and around the tumor, or might even affect normal neurological functions. Moreover, depending on the localization of the tumor, it might be inaccessible to get the tissue sample due to morbidity associated with the procedure. [12]. Furthermore, tissue biopsies can sometimes fail to predict the heterogeneity of the whole tumor. Therefore, histopathologic examination of representative tissue is required for the definitive diagnosis and grading of nervous system tumors [13]. Another diagnostic technique is the liquid biopsy, that might have some advantages versus tissue biopsy. It represents a simple and less invasive procedure that can provide similar information from certain body fluids (mainly blood) than what is usually obtained from a tissue biopsy sample [14]. Importantly, liquid biopsies could be obtained regularly over time, reflecting the real composition, the tumoral heterogeneity and the evolution of the tumor throughout time, allowing the monitoring of the tumor progression and therapy response.

In order to generate a more comprehensive understanding of the biological effects of new GBM therapies, it is critically important to use several animal models. Unquestionably, important insights into the pathogenesis of malignant gliomas, and the therapeutic mechanisms and effects of new therapies have been and will be gained through the study of chemically-induced, implanted tumor auto- or xenografts, or transgenic rodent tumor models. However, dogs and humans are the only species in which primary brain tumors are common [15]. Gliomas represent ~35% of all canine primary brain tumors, with high-grade oligodendroglioma and astrocytoma phenotypes accounting for ~70% of all canine gliomas [13]. Also, canine malignant gliomas (MG) exhibit the same pathology, molecular and cytogenetic abnormalities, as well as neuro-imaging characteristics [9, 16]. Dogs with MG develop significant signs of clinical dysfunction, including seizures, depressed or altered mental status, and motor dysfunction [17] which are also similar to those in humans. Canine gliomas are also treated using surgical, radiotherapeutic, and chemotherapeutic regimens similar to those used in humans. Unfortunately, patterns of survival for canines with MG are similar to those seen in people, with death relatively soon after diagnosis for those animals that are not euthanized at the time of diagnosis. Unlike implanted or chemically-induced tumors in

rodents, spontaneous tumors of the CNS in dogs occur in an immunocompetent host, are physically large and heterogeneous enough to facilitate testing and optimization of both experimental diagnostic and therapeutic devices and procedures that can be easily scaled for human patients.

The options for treating brain tumors include surgical removal, radiation therapy, chemotherapy, and palliative treatment of the symptoms. Research is currently under way to develop innovative techniques to improve the efficacy of the treatment and improve the prognosis of the patients. Our laboratory has been investigating irreversible electroporative (IRE) pulsed electrical field (PEF) technologies for the treatment of brain tumors [18]. These techniques employ microseconds-long electric pulses, applied with minimally invasive electrodes placed into targeted region, to generate electric fields that, depending on the strength of the electric filed applied, can either reversibly permeabilize the cell membrane, allowing treated cells to survive, or permanently disrupting the structure of the cell membrane, which causes cell death [19]. High Frequency Irreversible Electroporation (HFIRE) is the next generation of IRE technology which utilizes ultrashort (~0.5-2us) bipolar pulses that do not stimulate muscle contraction, mitigating the need for neuroparalytic agents [20] and creates a more electrically homogenous environment, resulting in more uniform ablations [21], and that have an ability to selectively ablate cancer cells at lower electric fields than healthy cells. We have demonstrated in our previous studies the safety and feasibility of stereotactic tumor ablation using lasers and pulsed electrical fields [22, 23], having a significant tumor size reduction without causing adverse events related to the treatment procedure.

Convection-enhanced delivery (CED) is another therapeutic technique of brain tumors in which our lab is working to improve. CED consists of the continuous administration of a fluid containing therapeutic agent under positive pressure via stereotactically placed small-caliber catheter(s) inserted into the brain [19, 24]. The CED technique has been investigated for its potential usefulness for the treatment of brain tumors, because it allows the direct delivery of large molecule therapeutics to the tumor that would not normally pass through the blood brain barrier (BBB) [25, 26]. Our lab had developed a multiport CED device arborizing catheter, the Convection Enhanced Thermotherapy Catheter System (CETCS), which allow us to of simultaneous co-delivering both fluids and light [27, 28]. One of the advantages of the photothermal capabilities of the CETCS is

that sublethal heating during infusion can increase the distribution volume of infusates by increasing fluid diffusion and convection, and reducing fluid viscosity [27, 28].

As all of these innovative treatment techniques involve invasive neurosurgical procedures, they are subject to a rigorous evaluations of safety to define the optimal therapeutic risk:benfit profile of each, and if adverse events occur, to understand what appropriate measures should be taken to mitigate morbidity. One pathophysiologic phenomenon that may contribute to the clinical symptom burden and adverse events in patients with brain tumors is glutamate excitotoxicity. Glutamate is the most abundant amino acid neurotransmitter in the brain (10000-12000 μmol/L), but its concentration in extracellular fluids is very low (0.5-2 μmol/L). Glutamate concentrations in plasma are 50-100 μmol/L [29]. This gradient is particularly important to maintain because excess glutamate in the extracellular fluid lead to overactivation of glutamate receptors which can initiate a number of deleterious consequences in a process called "excitotoxicity", including impairment of calcium buffering, generation of free radicals, and activation of the mitochondrial permeability transition, which ultimately results in cell death [30]. Studies have implicated excitotoxicity as a common pathophysiologic mechanism of disease in a variety of neuropathological conditions such as stroke, traumatic brain injury, neurodegenerative diseases, and GBM [29-31].

Gliomas have been shown to continuously secrete glutamate and therefore maintain a higher level of intra- and extracellular glutamate concentration than normal glial cells [32], contributing to cause the excitotoxicity. Extracellular glutamate levels in glioma were found to be 100 times higher than in healthy brain [33, 34], which lead to proliferation and invasion of glioma cells [35, 36]. The release of glutamate from glioma cells is caused by reduction of Na(+)-dependent glutamate transporters in conjunction with upregulation of cystine-glutamate exchange. The resulting glutamate release from glioma cells may contribute to tumor-associated necrosis and possibly to seizures in peritumoral brain tissue[37]. H-FIRE may contribute to excitotoxicity by the ablation of glioma cells and the neurons around the tumor, leading to a massive release of glutamate in the extracellular fluid. This is important to determine because depending on the concentration of glutamate released after H-FIRE treatment, it could potentially have therapeutic

effect affecting only the tumor cells, or may produce an adverse event that we have to manage simultaneously with the treatment to avoid the complication.

This work investigates how minimally invasive neurosurgical procedures that provide local access to the brain tissue and involve placement of small diameter needles, electrodes, or catheters into the brain for the purposes of obtaining a piece of tumor for diagnosis or delivering energy or drugs to kill tumor cells can be used safely and effectively for the management of patients with brain cancer. We evaluate the types and possible causes of complications associated with of these novel therapeutic procedures for the purposes of ultimately improving the outcome of patients of brain tumors. The specific objectives of the chapters of this work are:

1. **Chapter 2**- Determine if the stereotactic brain biopsy (SBB) technique is a representative and accurate method of diagnosis in dogs with brain tumors compared to the gold standard such as surgical resection or necropsy sampling.
    - Hypotheses: The diagnostic accuracy of SBB would be lower in dogs with gliomas than meningiomas, and that the diagnostic accuracy would be positively correlated with the number of SBB specimens obtained in each patient.
2. **Chapter 3-** Characterize the clinicopathologic responses to fiberoptic microneedles chronically implanted in the brain to evaluate the biocompatibility of the CECTCS microneedle component that comes into contact with the patient's brain tissue.
    - Hypotheses: FMD fragments chronically implanted in the brain of rats would: 1) not cause clinical evidence of brain disease; 2) result in neuropathological findings similar to those observed with other chronically implanted catheters in the central nervous system; and 3) not migrate outside of the calvarium.
3. **Chapters 4 and 5-** Determine if H-FIRE treatment of normal or glioma-bearing brains results in alterations in extracellular glutamate, and mechanistically characterize any such observed alterations in the context of glutamatergic signaling and metabolic pathways.
    - Hypotheses: H-FIRE will increase the glutamate concentration after treatment because of the cell membrane permeating mechanism and ablation effects of H-FIRE; glutamatergic excitotoxicity may be a mechanism of HFIRE induced cell death and BBB permeabilization and glutamate related gene expression in the tumor center of ablated tumors will be up-regulated compared to the tumor periphery.

REFERENCES

1. Arora, R.S., et al., *Age-incidence patterns of primary CNS tumors in children, adolescents, and adults in England.* Neuro Oncol, 2009. **11**(4): p. 403-13.
2. Batash, R., et al., *Glioblastoma Multiforme, Diagnosis and Treatment; Recent Literature Review.* Curr Med Chem, 2017. **24**(27): p. 3002-3009.
3. Shergalis, A., et al., *Current Challenges and Opportunities in Treating Glioblastoma.* Pharmacol Rev, 2018. **70**(3): p. 412-445.
4. Sarkaria, J.N., et al., *Is the blood-brain barrier really disrupted in all glioblastomas? A critical assessment of existing clinical data.* Neuro Oncol, 2018. **20**(2): p. 184-191.
5. Butler, M., et al., *MGMT Status as a Clinical Biomarker in Glioblastoma.* Trends Cancer, 2020. **6**(5): p. 380-391.
6. Miller, A.D., C.R. Miller, and J.H. Rossmeisl, *Canine Primary Intracranial Cancer: A Clinicopathologic and Comparative Review of Glioma, Meningioma, and Choroid Plexus Tumors.* Front Oncol, 2019. **9**: p. 1151.
7. Snyder, J.M., et al., *Canine Intracranial Primary Neoplasia: 173 Cases (1986–2003).* Journal of Veterinary Internal Medicine, 2006. **20**(3): p. 669-675.
8. Song, R.B., et al., *Postmortem evaluation of 435 cases of intracranial neoplasia in dogs and relationship of neoplasm with breed, age, and body weight.* J Vet Intern Med, 2013. **27**(5): p. 1143-52.
9. José-López, R., et al., *Clinical features, diagnosis, and survival analysis of dogs with glioma.* J Vet Intern Med, 2021. **35**(4): p. 1902-1917.
10. Rossmeisl, J.H., Jr., et al., *Invited review--neuroimaging response assessment criteria for brain tumors in veterinary patients.* Vet Radiol Ultrasound, 2014. **55**(2): p. 115-32.
11. Johnson, P.J., et al., *Relationship between histological tumor margins and magnetic resonance imaging signal intensities in brain neoplasia of dogs.* Journal of Veterinary Internal Medicine, 2022. **36**(3): p. 1039-1048.
12. Müller Bark, J., et al., *Circulating biomarkers in patients with glioblastoma.* British Journal of Cancer, 2020. **122**(3): p. 295-305.
13. Kani, Y., et al., *Diagnostic accuracy of stereotactic brain biopsy for intracranial neoplasia in dogs: Comparison of biopsy, surgical resection, and necropsy specimens.* J Vet Intern Med, 2019. **33**(3): p. 1384-1391.
14. Saenz-Antoñanzas, A., et al., *Liquid Biopsy in Glioblastoma: Opportunities, Applications and Challenges.* Cancers (Basel), 2019. **11**(7).
15. Dickinson, P.J., et al., *Canine spontaneous glioma: a translational model system for convection-enhanced delivery.* Neuro Oncol, 2010. **12**(9): p. 928-40.
16. Hicks, J., et al., *Canine brain tumours: a model for the human disease?* Vet Comp Oncol, 2017. **15**(1): p. 252-272.
17. LeCouteur, R.A. and S.J. Withrow, *Chapter 29 - Tumors of the Nervous System*, in *Withrow & MacEwen's Small Animal Clinical Oncology (Fourth Edition)*, S.J. Withrow and D.M. Vail, Editors. 2007, W.B. Saunders: Saint Louis. p. 659-685.
18. Davalos, R.V., I.L. Mir, and B. Rubinsky, *Tissue ablation with irreversible electroporation.* Ann Biomed Eng, 2005. **33**(2): p. 223-31.
19. Rossmeisl, J., *Maximizing Local Access to Therapeutic Deliveries in Glioblastoma. Part V: Clinically Relevant Model for Testing New Therapeutic Approaches*, in *Glioblastoma*, S. De Vleeschouwer, Editor. 2017: Brisbane (AU).
20. Arena, C.B., Sano, M.B., Rossmeisl, J.H., Caldwell, J.L., Garcia, P.A., Rylander, M.N.,

Davalos, R.V., *High- frequency irreversible electroporation (H-FIRE) for non-thermal ablation without muscle contraction.* Biomedical engineering online, 2011. **10**(1): p. 102.
21. Bhonsle, S.P., et al., *Mitigation of impedance changes due to electroporation therapy using bursts of high-frequency bipolar pulses.* Biomedical engineering online, 2015. **14**(Suppl 3): p. S3.
22. Latouche, E.L., et al., *High-Frequency Irreversible Electroporation for Intracranial Meningioma: A Feasibility Study in a Spontaneous Canine Tumor Model.* Technol Cancer Res Treat, 2018. **17**: p. 1533033818785285.
23. Rossmeisl, J.H., Jr., et al., *Safety and feasibility of the NanoKnife system for irreversible electroporation ablative treatment of canine spontaneous intracranial gliomas.* J Neurosurg, 2015. **123**(4): p. 1008-25.
24. Raghavan, R., et al., *Convection-enhanced delivery of therapeutics for brain disease, and its optimization.* Neurosurg Focus, 2006. **20**(4): p. E12.
25. Krauze, M.T., et al., *Reflux-free cannula for convection-enhanced high-speed delivery of therapeutic agents.* J Neurosurg, 2005. **103**(5): p. 923-9.
26. Ung, T.H., et al., *Convection-enhanced delivery for glioblastoma: targeted delivery of antitumor therapeutics.* CNS Oncol, 2015. **4**(4): p. 225-34.
27. Hood, R.L., et al., *Characterizing Thermal Augmentation of Convection-Enhanced Drug Delivery with the Fiberoptic Microneedle Device.* Engineering, 2015. **1**(3): p. 344-350.
28. Hood, R.L., et al., *Fiberoptic microneedle device facilitates volumetric infusate dispersion during convection-enhanced delivery in the brain.* Lasers Surg Med, 2013. **45**(7): p. 418-26.
29. Hawkins, R.A., *The blood-brain barrier and glutamate.* Am J Clin Nutr, 2009. **90**(3): p. 867S-874S.
30. Hawkins, R.A. and J.R. Vina, *How Glutamate Is Managed by the Blood-Brain Barrier.* Biology (Basel), 2016. **5**(4).
31. Andras, I.E., et al., *The NMDA and AMPA/KA receptors are involved in glutamate-induced alterations of occludin expression and phosphorylation in brain endothelial cells.* J Cereb Blood Flow Metab, 2007. **27**(8): p. 1431-43.
32. Ye, Z.C. and H. Sontheimer, *Glioma cells release excitotoxic concentrations of glutamate.* Cancer Res, 1999. **59**(17): p. 4383-91.
33. Marcus, H.J., et al., *In vivo assessment of high-grade glioma biochemistry using microdialysis: a study of energy-related molecules, growth factors and cytokines.* J Neurooncol, 2010. **97**(1): p. 11-23.
34. Roslin, M., et al., *Baseline levels of glucose metabolites, glutamate and glycerol in malignant glioma assessed by stereotactic microdialysis.* J Neurooncol, 2003. **61**(2): p. 151-60.
35. Takano, T., et al., *Glutamate release promotes growth of malignant gliomas.* Nature Medicine, 2001. **7**(9): p. 1010-1015.
36. Lyons, S.A., et al., *Autocrine glutamate signaling promotes glioma cell invasion.* Cancer Res, 2007. **67**(19): p. 9463-71.
37. Ye, Z.C., J.D. Rothstein, and H. Sontheimer, *Compromised glutamate transport in human glioma cells: reduction-mislocalization of sodium-dependent glutamate transporters and enhanced activity of cystine-glutamate exchange.* J Neurosci, 1999. **19**(24): p. 10767-77.

CHAPTER 2. DIAGNOSTIC ACCURACY OF STEREOTACTIC BRAIN BIOPSY FOR CANINE INTRACRANIAL NEOPLASIA: COMPARISON OF BIOPSY, SURGICAL RESECTION, AND NECROPSY SPECIMENS

 Kani Y, Cecere TE, Lahmers K, LeRoith T, Zimmerman KL, Isom S, Hsu FC, Debinksi W, Robertson JL, Rossmeisl JH. Diagnostic accuracy of stereotactic brain biopsy for intracranial neoplasia in dogs: Comparison of biopsy, surgical resection, and necropsy specimens. J Vet Int Med 2019; 33(3):1384-1391.

ABSTRACT

Background: Stereotactic brain biopsy (SBB) is a technique that allows for definitive diagnosis of brain lesions. There is little information regarding the diagnostic utility of SBB in dogs with intracranial diseases.

Objectives: To investigate the diagnostic accuracy (DA) of SBB in dogs with brain tumors.

Animals: 31 client-owned dogs that underwent SBB followed by surgical resection or necropsy examinations.

Methods: Retrospective observational study. Two pathologists blinded to SBB and reference standard diagnoses reviewed histologic specimens and typed and graded tumors according to World Health Organization (WHO) and revised canine glioma classification criteria. Agreement between tumor type and grade from SBB were compared to reference standards and assessed with kappa statistics. Patient and technical factors associated with agreement were also examined.

Results: SBB were obtained from 24 dogs with gliomas and 7 with meningiomas. Tumor type agreement between SBB and the reference standard was observed in 30/31 cases (Kappa= 0.95). Diagnostic concordance was perfect for meningiomas. Grade agreement among gliomas was observed in 18/23 cases (Kappa=0.47). SBB underrepresented the reference standard glioma grade in cases with disagreement. The DA of SBB was 81%, with agreement noted in 56/69 biopsy samples. Smaller tumors and fewer SBB obtained were significantly associated with diagnostic discordance.

Conclusions and Clinical Importance: The DA of SBB readily allows for the diagnosis of common types of brain tumors. Although glioma grade discordance was frequent, diagnoses

obtained from SBB are sufficient to currently inform therapeutic decisions. Multiple SBB should be collected to maximize the DA.

INTRODUCTION

Advancements in diagnostic imaging, particularly magnetic resonance imaging (MRI), have revolutionized the management of many veterinary intracranial disorders predominantly by providing information that complements historical and clinical findings and allows for the generation of a refined list of differential diagnoses. However, all of the currently available imaging modalities are sufficiently unreliable to allow for the definitive diagnosis of most intracranial disorders that are commonly encountered in neurology practice.[1-4] As potential treatments and prognoses can differ substantially among the differential diagnoses generated in an individual patient based on clinical and imaging data, this diagnostic uncertainty can have profound implications on patient management. For example, in one study of dogs with focal intra-axial brain lesions on MRI, as many as 47% of cerebrovascular accidents were misdiagnosed as gliomas, and up to 12% of gliomas misclassified as strokes.[2]

Given the current limitations of diagnostic imaging, acquisition of representative samples of brain tissue that allow a neuropathologist to provide a definitive diagnosis remains integral to informing best clinical practices regarding the selection of therapy for patients with brain disease. To meet this diagnostic need, minimally invasive stereotactic methods were introduced into human neurosurgical practice over a century ago and have evolved continuously since then. To date, stereotactic brain biopsy (SBB) remains one of the most commonly performed stereotactic procedures.[3,4] Diagnoses sufficient to guide therapeutic decision making are obtained in 95% of humans in which SBB is performed, with a low risk of associated adverse events.[4]

There are few reports describing the clinical utility of SBB procedures performed in dogs with intracranial diseases.[5,6] Specific measures of the diagnostic utility of histopathological samples obtained using biopsy techniques include the diagnostic yield (DY), which is the proportion of biopsies producing a specific pathological diagnosis. The DY is calculated by dividing the number of biopsies producing specific pathological diagnosis by the total number of total biopsies performed. In dogs with intracranial lesions, the DY of SBB has been reported to be 95%.[5] The diagnostic accuracy (DA) examines the rate of concordance between samples obtained by biopsy and the final pathological diagnosis obtained by a reference standard method, such as surgical resection or necropsy examination. The DA is calculated by dividing the number of biopsies giving same diagnosis as surgical or necropsy specimens by total biopsies

performed. To date, there is very little data available regarding the DA of SBB in dogs with naturally occurring brain diseases.[6]

The objectives of this study were to determine if the neuropathologic diagnosis obtained by SBB, using the tumor type and grade as diagnostic endpoints, was an accurate representation of the entire lesion when compared to reference standard surgical resection or necropsy specimens, and to identify any risk factors associated with diagnostic discordance. We hypothesized that the DA of SBB would be lower in dogs with gliomas than meningiomas, and that the DA would be positively correlated with the number of SBB obtained in each patient.

MATERIALS AND METHODS

Study Design

Retrospective observational study.

Dog and tumor characteristics

The medical records of 31 dogs that underwent SBB followed by open craniotomy and surgical mass resection (SR) or necropsy examination (NE) between June of 2008 and June of 2018 were identified by searching a veterinary clinical trial database. Patient data were entered into the database prospectively during clinical trial participation. For the purposes of this study, information extracted from the database included the signalment, the lesion side and location in the brain, T2W-volume of the target lesion at the time of SBB, the number of SBB attempted, the number of SBB obtained, the number of biopsy trajectories used during the procedure, and the number of days elapsed between the performance of the SBB and the subsequent reference standard method (SR or NE).[5] All dogs in this study underwent SBB to further evaluate newly MRI-diagnosed brain mass lesions associated with clinical signs of intracranial disease. A single clinician performed all SBB procedures in anesthetized dogs using a previously described frame-based technique.[5]

Neuropathological review and tumor classification

All archived slides representing samples obtained from the brain from each dog's case were collected and anonymized. A random number generator (SAS v. 9.4, SAS Institute, Cary, NC, USA) was used to assign a unique numeric identifier to all of the slides belonging to an

individual dog. Anonymized slide labels contained the unique numeric identifier assigned, as well as the type of staining procedure used on the slide. Anonymized slides were then assembled into two sets: a set containing SBB slides from all dogs, and another set containing all SR/NE slides from all dogs. Hematoxylin and eosin (H&E) stained slides were available for all cases in both sets. When available, slides stained immunohistochemically with glial fibrillary acidic protein (GFAP; Dako[a] polyclonal, 1:150), vimentin (Dako clone V9, 1:300), or oligodendrocyte transcription factor 2 (Olig-2; Millipore polyclonal, 1:100) were included for each case in each set.[7]

Each slide set was then distributed to two veterinary pathologists that were not involved in generating the original pathology reports contained in medical records. From the slide material provided for each case in each set, pathologists were asked to provide a neuropathologic diagnosis, and if the assigned diagnosis was neoplastic, that tumors initially be classified and graded according to World Health Organization (WHO) criteria.[8] Two pathologists were later tasked with reclassifying glial tumors following the recent release of the revised canine classification criteria, in which gliomas are graded in a binary fashion (high- versus low-grade).[9] During the review process, pathologists were asked to provide specific reasons for any samples that were determined to be non-diagnostic, and any comments regarding the samples that influenced their diagnostic conclusions. At least six weeks lapsed between a pathologist's review of each of the slide sets. In the event of diagnostic discordance between the two examining pathologists, the histopathologic diagnosis coded in the original pathology report for the specimen in question was used to arrive at a majority opinion.

Statistical Analyses

Means, standard deviations, medians, and ranges were calculated for continuous characteristics. Counts and proportions were calculated for discrete characteristics. To compare the median tumor volume or the median number of biopsy trajectories between dogs with meningiomas and gliomas, the Kruskal-Wallis test was used. The diagnostic concordance of tumor type or tumor grade between SBB and the reference standard was calculated using Cohen's Kappa statistics and tested using the McNemar test. The two-sample t-tests were used for the comparisons of normally distributed patient characteristics between the two concordance groups (agreement vs. no agreement) and Kruskal-Wallis tests were used for the comparisons of non-normally distributed

patient characteristics. For discrete patient characteristics, Fisher's exact tests were used. Statistical analyses were completed using SAS software version 9.4 (SAS Institute, Cary, NC, USA). P-values < 0.05 were considered significant.

RESULTS

Dog and tumor characteristics

A total of 31 dogs were included in the study. The median age at diagnosis by SBB was 9 years (range, 6 to 12 years). There were 14 spayed females, 16 neutered males, and one intact male. The median body weight was 20 kg (range, 7 to 43 kg). Fifteen breeds of dogs were represented including mixed breeds (n=8), Boston terrier (n=6), Boxer (n=4), American Staffordshire terrier (n=2), Labrador retriever (n=2) and one each of the following: Beagle, Bull terrier, French Bulldog, German Shepherd, Golden retriever, Miniature Schnauzer, Rat terrier, Rottweiler, and Siberian Husky.

All tumors were located in the prosencephalon with 29 occurring on or in the cerebral hemispheres and 2 being located in the thalamus. Fourteen tumors were located on the left side of the brain, 15 on the right side, and 2 on the midline. The median tumor volume was 2.9 cm^3 (range, 0.55 to 12.3 cm^3). The median volume of meningiomas was significantly greater than the median volume of gliomas (p=0.03; Table 2-1).

Neuropathological results and diagnostic agreement

Reference standard (SR, n=14 or NE, n=17) WHO neuropathological diagnoses included 10 astrocytomas (n=1 Grade II; n=1 Grade III; and n=8 Grade IV), 13 oligodendrogliomas (n=4 Grade II; n=9 Grade III), one Grade III oligoastrocytoma (undefined) glioma, and 7 meningiomas (n=4 Grade I; n=3 Grade II). Using the revised canine glioma classification criteria, all tissue specimens initially graded as WHO grade II gliomas were reported as low-grade tumors, and all WHO Grade III and IV tumors as high-grade gliomas by pathologists.

A total of 69 individual biopsy samples were obtained from the 31 dogs. The median number of SBB obtained was 2 (range, 1 to 4), and was not different between meningiomas or gliomas (p=0.26; Table 2-1). A significantly larger (p=0.003; Table 2-1) number of biopsy trajectories was used in dogs with meningiomas than gliomas. A total of 4/69 SBB samples were

non-diagnostic, resulting in a DY of 94.2% for the SBB procedure. Non-diagnostic biopsies were only obtained from patients with glial tumors in this study. Non-diagnostic biopsy diagnoses included normal brain tissue, hemorrhage, astrogliosis, necrosis, and amorphous eosinophilic material. The median number of days between SBB and performance of the reference standard diagnostic method was 75 days (range, 1 to 372 days).

Table 2-1. Tumor and Biopsy Technical Factor Comparisons Between Tumor Types

	Tumor Type		p-value
	Glioma	**Meningioma**	
N	24	7	
Median Tumor Volume (cm^3)	2.8 (0.55-12.3)	5.3 (2.9-10.3)	0.03*
Number of Biopsy Trajectories			0.003*
1	20 (83.3%)	2 (28.6%)	
2	4 (16.7%)	2 (28.6%)	
3	0	3 (42.9%)	
Number of Biopsies Obtained			0.26
1	6 (25.0%)	0	
2	11 (45.8%)	3 (42.9%)	
3	6 (25.0%)	3 (42.9%)	
4	1 (4.2%)	1 (14.3%)	

Table 2-1. Key

p-values are exact tests for categorical measures, t-tests when means are presented, and Kruskal-Wallis test when medians are presented

*Statistically significant ($p<0.05$)

The overall DA, using the WHO grading classification scheme, was 81%, with diagnostic agreement noted between SBB and the reference standard method in a total of 56/69 biopsy samples. Diagnostic concordance of tumor type between SBB and the reference standard was observed in 30/31 cases (Kappa=0.95). None of the patient characteristics examined (breed, sex, age, body weight), reference standard methods (surgery or necropsy), SBB variables (number of

biopsy trajectories, biopsies attempted, biopsies obtained, non-diagnostic biopsies), or tumor features (lesion side, location, volume, tumor type), significantly influenced tumor type concordance between SBB and the reference standard ($p > 0.05$).

Tumor grade agreements between SBB and reference standard methods were assessed for 30 cases, as a tumor grade could not be determined for one SBB glioma case (Table 2-2). Universal tumor type and grade agreement was found for all 7 meningiomas. The overall diagnostic concordance for all evaluable tumors using WHO classification was 80% (24/30 cases; Kappa= 0.73). Diagnostic grade concordance using the revised canine glioma classification was observed in 78% of cases (18/23 cases; Kappa = 0.47), and glioma grading agreement between WHO and revised canine glioma schema were not significantly different (McNemar p=0.56). In 6/6 cases of WHO and 4/5 cases revised canine glioma grading discordance, SBB underestimated the tumor grade when compared to the reference standard. Smaller lesion volume was significantly associated with diagnostic discordance (Table 2-2) in both WHO and revised canine glioma classification systems. In addition, fewer number of biopsies attempted (p=0.006) and fewer number of biopsies obtained (p=0.004), were factors that were significantly associated with tumor grade discordance using the WHO system (Table 2-2).

DISCUSSION

In this study, the DY of SBB was 94% and the overall DA 81%. These findings are similar to previously published studies of dogs and humans undergoing frame-based SBB, which report DY for neoplastic lesions ranging from 89-99% and DA of 63-90%.[5,6,10-16] In both human and veterinary medicine, improvements in the DY and DA of brain biopsy have evolved in parallel with clinician experience, as well as with diagnostic imaging and surgical technologies.[5,6,10-16] To date, there have only been two studies reporting the DA of needle biopsy in dogs with naturally occurring brain tumors. One investigation using a free-hand biopsy technique resulted in a DA of 13%, with diagnostic tumor type agreement noted between biopsy and necropsy in 1/8 cases.[15] Another study using an SBB procedure reported a DA of 91% (20/22 cases) in dogs with brain tumors.[6] Neither of these previous studies in dogs included analyses of tumor grade as a component of diagnostic concordance. Here we report an accuracy of 97% (30/31 cases) for determination of tumor type. The excellent agreement between SBB and the reference standard

tumor type diagnoses in this, and other studies, provides additional evidence that SBB is a sufficiently accurate technique to provide definitive histologic diagnoses of brain tumors and subsequently guide patient care.[6] As meningiomas and gliomas account for 75-90% of all canine primary brain tumors, the cohort of dogs reported here is an appropriate representation of potential candidates for SBB encountered in clinical practice.[6,17]

Diagnostic agreement for tumor type and grade was perfect for all meningioma cases in this cohort, although no attempt was made to examine concordance with respect to meningioma histologic subtypes. As hypothesized, the DA of gliomas was lower than that of meningiomas. This finding is not unexpected given that meningiomas were significantly larger than gliomas, and more biopsy trajectories were used in meningioma cases. Although the number of biopsies obtained was not statistically different between meningiomas and gliomas, usage of a higher number of biopsy trajectories may improve diagnostic agreement by providing a superior geographic representation of tumor histology.

All of the diagnostic discordance observed in this study occurred during evaluation of glial tumors, and the majority of disagreements were attributable to tumor grading. Glioma grade agreement was moderate and not significantly different between both grading systems (17/23 WHO graded cases and 18/23 revised canine cases). Notably, SBB frequently underestimated the glioma grade compared to SR or NE. The difference in the grade concordance between systems is likely explained because the WHO glioma grading system has 4 categories, while the revised canine classification grades in a binary fashion (high or low). Thus, it is not unexpected that more disagreements were noted using the WHO grade system. Pathologists in this study commented that the absence of the hallmark morphologic feature of necrosis in SBB specimens often precluded assignment of a grade 4 astrocytoma or grade 3 oligodendroglioma (high-grade gliomas) diagnosis.[9] This may represent a form of sampling bias, as the neurosurgeon performing SBB in this study intentionally avoided necrotic tumor regions given that obtaining biopsies from necrotic areas accounts for a substantial proportion of non-diagnostic samples in canine and human studies of SBB.[5,11,13,15] Phenotypic heterogeneity within gliomas is well recognized to present diagnostic challenges to human and veterinary neuropathologists, especially when considering the sample size limitations inherent to SBB.[9,15] Our findings further support usage of revised canine glioma system to streamline and standardize canine glioma diagnosis.

Factors that were identified to significantly influence glioma grade discordance in this study were the lesion volume, number of biopsies attempted, and the number of biopsies obtained. Gliomas in which grade discordance was noted were significantly smaller than those in which there was grade agreement. Previous investigations of SBB in humans and dogs have indicated that SBB of smaller lesions may result in lower diagnostic agreement for numerous reasons such as targeting inaccuracies, mechanical deformation of the target at the time of the biopsy, limited quantity or quality of biopsies obtained, and higher probability of obtaining biopsies outside the tumor or at its boundaries.[5,10,13,15] One human study also demonstrated that SBB of very large gliomas (>50 cm^3) resulted in biopsy samples that were less representative of the entire lesion because of the extensive areas of necrosis and extreme intratumoral heterogeneity.[13]

The number of biopsies attempted and obtained were also significant variables that affected diagnostic accuracy of SBB in this and other studies, and are often inherently related to the lesion volume.[5] The median number of biopsies obtained in cases of diagnostic discordance in this cohort was one, which highlights the importance of obtaining multiple biopsy samples to improve the diagnostic accuracy of SBB. Performance of a geographic core biopsy technique represents one possible solution for optimizing the DA of SBB by obtaining multiple samples along a singular biopsy trajectory.

Several limitations of this report may also have impacted our agreement. First, methods to minimize interobserver variability between pathologists classifying tumors were not included in the study design. Although pathologists participating in this study all have neuropathological experience with canine brain tumors and SBB, similar to the results reported here, agreement among experts reviewing canine and human glioma histomorphology and grade has been previously reported as moderate.[5,9,18] Incorporation of joint training and multiple specimen review sessions for pathologists have been shown to improve the DA and should be considered in future studies.[19] All of the dogs in this report received interventions including stereotactic radiotherapeutic, molecularly targeted biological, and other ablative therapies between the time SBB and reference standard tissue samples were collected.[20-22] Tumor phenotypes may change over time as a result of natural tumor progression or secondary to treatments administered.[11,13,15,21] Although time elapsed between SBB and the reference standard was not shown to significantly influence diagnostic concordance in this report, the median time elapsed between SBB and reference standard diagnosis cases with glioma grade discordance (126 days) was nearly twice as

long as cases demonstrating agreement (68 days). In addition, the only disagreement in tumor type diagnosis observed in this study also had the longest delay (372 days) between SBB and necropsy.

CONCLUSIONS

The DA of SBB readily allows for the definitive diagnosis of different types of common brain tumors in dogs. Agreement between SBB and reference standard methods for glioma grading was moderate, with SBB frequently underestimating the glioma grade. However, given the currently unknown influences of tumor grade on the prognosis of dogs with gliomas, SBB provides sufficient information to rationally guide therapeutic decisions in dogs with brain tumors. Multiple biopsies should be obtained to maximize the diagnostic accuracy of SBB.

Acknowledgements

This study was supported by grants from the National Institutes of Health (R01CA139099/CA/NCI NIH HHS and P01CA207206/CA/NCI NIH HHS).

Institutional Animal Care and Use Committee (IACUC) Declaration

The study was conducted in accordance with the guidelines of the Virginia Tech Institutional Animal Care and Use Committee (protocols 17-011, 17-203, 16-017, 15-221, 14-235, 12-014, and 08-218).

REFERENCES

1. Wolff CA, Holmes SP, Young BD, et al. Magnetic resonance imaging for the differentiation of neoplastic, inflammatory, and cerebrovascular brain disease in dogs. *J Vet Int Med* 2012;26:589-597.
2. Cervera V, Mai W, Vite CH, et al. Comparative magnetic resonance imaging findings between gliomas and presumed cerebrovascular accidents in dogs. *Vet Radiol Ultrasound* 2011;52:33-40.
3. Friedman WA, Sceats DJ, Nestok BR, Ballinger WE. The incidence of unexpected pathological findings in an image-guided biopsy series: a review of 100 consecutive cases. *Neurosurgery* 1989;25:180-184.
4. Apuzzo ML, Chandrasoma PT, Cohen, et al. Computed imaging stereotaxy: experience and perspective related to 500 procedures applied to brain masses. *Neurosurgery* 1987;20:930-937.
5. Rossmeisl JH, Andriani RT, Cecere TE, et al. Frame-based stereotactic biopsy of canine brain masses: technique and clinical results in 26 cases. *Front Vet Sci* 2015;2:20.
6. Koblik PD, LeCouteur RJ, Higgins RJ, et al. CT-guided brain biopsy using a modified Pelorus Mark III stereotactic system: experience with 50 dogs. *Vet Radiol Ultrasound* 1999;40:434-440.
7. Rossmeisl Jr. JH, Pineyro P, Sponenberg DP, et al. Clinicopathologic features of intracranial central neurocytomas in 2 dogs. *J Vet Int Med* 2012;26:186-191.
8. Louis DN, Ohgaki H, Wiestler OD, et al. The 2007 WHO classification of tumors of the central nervous system. *Acta Neuropathol* 2007;114:97-109.
9. Koehler JW, Miller AD, Miller CR, et al. A revised diagnostic classification of canine glioma: Towards validation of the canine glioma patient as a naturally occurring preclinical model for human glioma. *J Neuropathol Exp Neurol* 2018; 77:1039-1054.
10. Moissonnier P, Blot S, Devauchelle P, et al. Stereotactic CT-guided brain biopsy in the dog. *J Small Anim Pract* 2002; 43:115–123.
11. Aker FV, Hakan T, Karadereler S, et al. Accuracy and diagnostic yield of stereotactic biopsy in the diagnosis of brain masses: comparison of results of biopsy and resected surgical specimens. *Neuropathol* 2005; 25: 207-213.

12. Owen CM, Linskey ME. Frame-based stereotaxy in a frameless era: current capabilities, relative role, and the positive- and negative predictive values of blood through the needle. *J Neurooncol* 2009; 93:139-149.
13. Woodworth G, McGirt MJ, Samdani, et al. Accuracy of frameless and frame-based image-guided stereotactic brain biopsy in the diagnosis of glioma: comparison of biopsy and open resection specimen. *Neurol Res* 2005; 27: 358-362.
14. Callovini GM, Telera S, Sherkat S, et al. How is stereotactic brain biopsy evolving? A multicentric analysis of a series of 421 cases treated in Rome over the last sixteen years. *Clin Neurol Neurosurg* 2018; 174:101-107.
15. Chandrasoma PT, Smith MM, Apuzzo ML. Stereotactic biopsy in the diagnosis of brain masses: comparison of results of biopsy and resected surgical specimen. *Neurosurgery* 1989; 24:160-165.
16. Harari J, Moore MM, Leathers CW, et al. Computed tomographic- guided, free-hand needle biopsy of brain tumors in dogs. *Prog Vet Neurol* 1994; 4:41-44.
17. Song RB, Vite CH, Bradley CW, et al. Postmortem evaluation of 435 cases of intracranial neoplasia in dogs and relationship of neoplasm with breed, age, and body weight. *J Vet Int Med* 2013; 27: 1143-1152.
18. van den Bent MJ. Interobserver variation of the histopathological diagnosis in clinical trials on glioma: A clinician's perspective. *Acta Neuropathol* 2010; 120:297-304.
19. Coons SW, Johnson PC, Scheithauer BW, et al. Improving diagnostic accuracy and interobserver concordance in the classification and grading of primary gliomas. *Cancer* 1997; 79:1381-1393.
20. Debinski W, Dickinson P, Rossmeisl JH, et al. New agents for targeting of IL-13RA2 expressed in primary human and canine brain tumors. *PLoS ONE* 2013; 8: e77719.
21. Rossmeisl JH, Garcia PA, Pancotto TE, et al. Safety and feasibility of the NanoKnife system for irreversible electroporation ablative treatment of canine spontaneous intracranial gliomas. *J Neurosurg* 2015; 123: 1008-1025.
22. Rossmeisl JH, Hall-Manning K, Robertson JL, et al. Expression and activity of the urokinase plasminogen activator system in canine primary brain tumors. *Onco Targets Ther* 2017; 10: 2077-2085.

23. Jain D, Sharma M, Sarkar C, et al. Correlation of diagnostic yield of stereotactic brain biopsy with number of biopsy bits and site of the lesion. *Brain Tumor Pathol* 2006 23**:**71-75.

Table 2-2. Factors Associated with Tumor Grade Agreement Between World Health Organization and Revised Canine Glioma Classification Criteria

	WHO Grades Agree, n= 30 cases			Canine Grades Agree, n= 23 cases		
	No	**Yes**	**p-value**	**No**	**Yes**	**p-value**
N	6 (20%)	24 (80%)		5 (21.7%)	18 (78.3%)	
Age (years), mean (sd)	8.8 (2.1)	9.1 (1.7)	0.72	9.2 (2.2)	8.7 (1.7)	0.61
Body Weight (kg), mean (sd)	20.5 (7.6)	22.0 (11.7)	0.77	18.0 (7.5)	21.2 (10.9)	0.55
Lesion Volume (cm^3), mean (sd)	1.2 (0.7)	4.2 (3.0)	0.0001*	1.4 (0.9)	3.4 (3.0)	0.02*
Sex			0.49			0.31
Female spayed	4 (30.8%)	9 (69.2%)		2 (22.2%)	7 (77.8%)	
Male neutered	2 (12.5%)	14 (87.5%)		2 (15.4%)	11 (84.6%)	
Male	0	1 (100.0%)		1 (100.0%)	0	
Reference Standard Method			0.18			0.27
Surgery	1 (7.1%)	13 (92.9%)		0	7 (100.0%)	
Necropsy	5 (31.3%)	11 (68.8%)		5 (31.3%)	11 (68.8%)	
Number Biopsy Trajectories			0.26			0.54
1	6 (28.6%)	15 (71.4%)		5 (26.3%)	14 (73.7%)	
2	0	6 (100.0%)		0	4 (100.0%)	
3	0	3 (100.0%)		0	0	
Number Biopsies Attempted			0.006*			0.15

	WHO Grades Agree, n= 30 cases			Canine Grades Agree, n= 23 cases		
	No	**Yes**	**p-value**	**No**	**Yes**	**p-value**
1	4 (80.0%)	1 (20.0%)		3 (60%)	2 (40%)	
2	2 (15.4%)	11 (84.6%)		1 (10%)	9 (90%)	
3	0	9 (100.0%)		1 (16.7%)	5(83.3%)	
4	0	3 (100.0%)		0	2 (100.0%)	
Number Biopsies Obtained			0.004*			0.07
1	4 (80.0%)	1 (20.0%)		3 (60.0%)	2 (40.0%)	
2	2 (14.3%)	12 (85.7%)		1 (9.1%)	10(90.9%)	
3	0	9 (100.0%)		1 (16.7%)	5 (83.3%)	
4	0	2 (100.0%)		0	1 (100.0%)	
Number Non-diagnostic Biopsies			0.56			1.00
1	0	4 (100.0%)		0	3 (100.0%)	
0	6 (23.1%)	20 (76.9%)		5 (25%)	25 (80%)	
Lesion Side			0.25			0.64
Left	5 (35.7%)	9 (64.3%)		3 (27.3%)	8 (72.7%)	
Right	1 (7.1%)	13 (92.9%)		2 (16.7%)	10 (83.3%)	
Midline	0	2 (100.0%)		0	0	
Tumor Type (Reference Standard)			0.41			0.052
Astrocytoma	2 (20.0%)	8 (80.0%)		0	10 (100.0%)	

	WHO Grades Agree, n= 30 cases			Canine Grades Agree, n= 23 cases		
	No	**Yes**	**p-value**	**No**	**Yes**	**p-value**
Oligodendroglioma	4 (33.3%)	8 (66.7%)		5 (41.7%)	7 (58.3%)	
Glioma undefined/Oligoastrocytoma	0	1 (100.0%)		0	1 (100.0%)	
Meningioma	0	7 (100.0%)		NA	NA	
WHO Tumor Grade (Reference Standard)			0.16			0.14
1	0	4 (100.0%)		0	0	
2	0	8 (100.0%)		1 20%)	4 (80%)	
3	4 (40.0%)	6 (60.0%)		4 (40.0%)	6 (60.0%)	
4	2 (25.0%)	6 (75.0%)		0	8 (100.0%)	
Canine Glioma Grade (Reference Standard)			NA			1.00
Low	NA	NA		1 (20%)	4 (80%)	
High	NA	NA		4 (22.2%)	14 (77.8%)	
Time (days) from SBB to Reference Standard, median (IQR)	110.5 (45.0)	25.0 (157.0)	0.25	126.0 (61.0)	68.5 (158.0)	0.26

Table 2 Key

IQR= interquartile range

NA= not applicable

WHO= World Health Organization

p-values are exact tests for categorical measures, t-tests when means are presented, and Kruskal-Wallis test when medians are presented

*Statistically significant ($p<0.05$)

CHAPTER 3. BIOCOMPATIBILITY OF THE FIBEROPTIC MICRONEEDLE DEVICE CHRONICALLY IMPLANTED IN THE RAT BRAIN

 Kani Y, Hinckley J, Robertson JL, Mehta JM, Rylander CG, Rossmeisl JH. Biocompatibility of the fiberoptic microneedle device chronically implanted in the rat brain. Res Vet Sci 2022; 143: 74-80.

ABSTRACT

The fiberoptic microneedle device (FMD) is a fused-silica microcatheter capable of co-delivery of fluids and light that has been developed for convection-enhanced delivery and photothermal treatments of glioblastoma. Here we investigate the biocompatibility of FMD fragments chronically implanted in the rat brain in the context of evaluating potential mechanical device failure. Fischer rats underwent craniectomy procedures for sham control (n=16) or FMD implantation (n=16) within the brain. Rats were examined daily after implantation, and at 14, 30, 90, and 180 days after implantation were evaluated via computed tomography of the head, hematologic and blood biochemical profiling, and histologic examinations. Clinical signs of illness and distant implant migration were not observed, and blood analyses were not different between control and FMD implanted groups at any time. Mild inflammatory and astrogliotic reactions localized to the treatment sites within the brain were observed in all groups, more robust in FMD implanted groups compared to controls at days 30 and 90, and decreased in severity over day 90-180 of the study. One rat developed a chronic, superficial surgical site pyogranuloma attributed to the FMD silica implant. Chronically implanted FMD fragments were well tolerated clinically and resulted in anticipated mild, localized brain tissue responses that were comparable with other implanted biomaterials in the brain.

Keywords: Biocompatibility, fiberoptic microneedle device, rat brain, convection enhanced delivery.

INTRODUCTION

Convection-enhanced delivery (CED) is the continuous administration of a fluid containing therapeutic agent under positive pressure via stereotactically placed small-caliber catheter(s) inserted into the brain.[1,2] The CED technique has been investigated for its potential usefulness for the treatment of brain tumors, because it allows the direct delivery of large molecule therapeutics to the tumor that would not normally pass through the blood brain barrier (BBB).[3-6] CED can also increase the distribution volume (V_d) of the drug in the brain tissue orders of magnitude over what can be achieved by simple diffusion without significantly increasing intracranial pressure.[2]

One of the major limitations of CED is the inability to consistently distribute therapeutic agents to the entire, biophysically heterogeneous, target brain or tumor volume.[1,6,7] It has been shown that the V_d of CED infusates can vary depending on the tumor's location in the brain as well as it's microenvironmental characteristics. For example, CED infusions performed in proximity to the ventricular system have a propensity to result in drug leakage into the low-pressure ventricles and drugs may pool in necrotic tumor regions preventing distribution to viable cancer cells.[6,7] Other major determinants of the efficacy of CED are physical features of the catheter. Historically, catheter clogging, infusate reflux or backflow, and air bubble formation have complicated complete treatment of brain tumors with CED.[6,8] To overcome reflux, catheters have been designed to incorporate reflux-preventing properties such as a 'step change', in which the diameter of the catheter narrows the distal tip of the catheter.[3] These reflux preventing catheters have been shown to be capable of delivering CED infusates at high flow rates without reflux in normal and diseased brain tissues.[1,3,6]

Additional improvements to CED approaches for brain tumors have manifested as multiport catheters capable of delivering high volumes of therapeutics through a single insertion portal.[9,10] One example of such a multiport CED device is our proprietary arborizing catheter, the Convection Enhanced Thermotherapy Catheter System (CETCS). The CETCS consists of a rigid primary cannula which contains up to seven ports, each of

which houses an individual fiberoptic microneedle device (FMD; Figure 1). Each FMD is a light-guiding, fused silica capillary tube capable of simultaneous co-delivering both fluids and light.[11,12] The photothermal capabilities of the CETCS offer advantages over existing multiport CED catheter systems in that sublethal heating during infusion can increase the V_d of infusates by increasing fluid diffusion and convection, and reducing fluid viscosity.[11] CETCS hyperthermic applications include laser interstitial thermotherapy for tumor ablation, augmentation of the cytotoxicity of chemotherapeutic agents, or prevention of tumor cell seeding of needle track.[12-15]

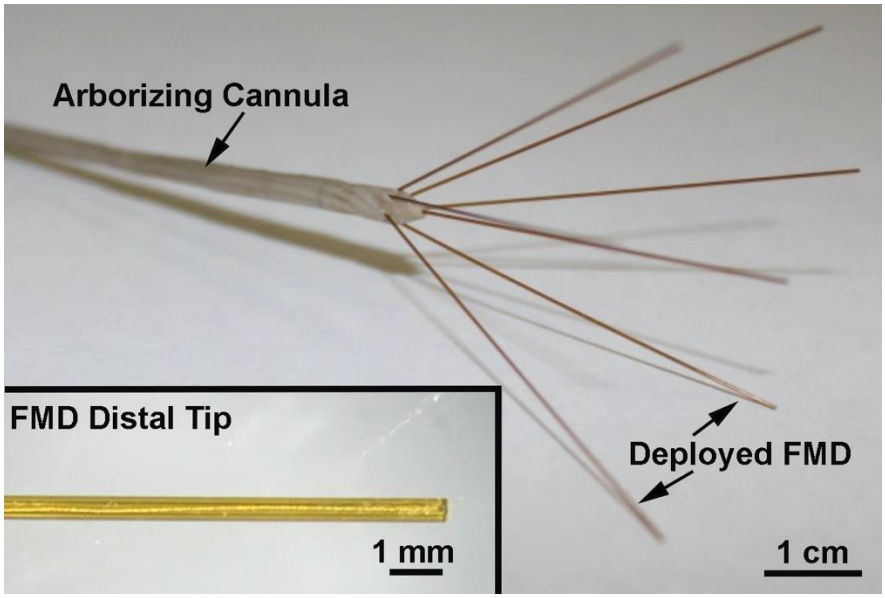

Figure 3-1. Convection Enhanced Thermotherapy Catheter System. It consists of a primary arborizing cannula from which up to six individual fiberoptic microneedle devices (FMD) can be deployed. Each FMD (inset) is constructed from small caliber fused-silica capillary tubing and capable of co-delivering fluids and light.

Possible adverse events associated with mechanical failure of the CETCS system would be breakage of a FMD deep within the brain parenchyma or subsequent migration of the broken FMD fragment outside of the brain. To evaluate the *in vivo* effects of these potential complications, the objectives of this study were to characterize the clinicopathologic responses to microneedle fragments chronically implanted in the brain of rats and determine if systemic FMD migration occurred in these rodents. We hypothesized that FMD fragments chronically implanted in the brain of rats would: 1) not cause clinical

evidence of brain disease; 2) result in neuropathological findings similar to those observed with other chronically implanted catheters in the central nervous system;[16] and 3) not migrate outside of the calvarium.

MATERIALS AND METHODS

Study Design

Thirty-two adult male Fisher rats were randomly assigned to sham control (n=16; FMD inserted into brain tissue and then withdrawn) and FMD implanted treatment groups (n=16; FMD fragment implanted within brain parenchyma).[11,12] Surgical treatments were performed on study day 0. At 14, 30, 90 and 180 days following surgical treatments, 4 each of FMD implanted and sham control rats were weighed, had a complete blood count and biochemical profile performed on peripheral blood and then were euthanized by barbiturate overdosage. A post-mortem micro-computed tomographic (mCT) imaging examination of the head and necropsy examination were then performed. The study was performed in accordance with the principles of Guide for the Care and Use of Laboratory Animals and was approved by the Institutional Animal Care and Use Committee of Virginia Tech (IACUC #19-245).

Craniectomy and FMD Insertion into the Brain

On day 0, the animals were weighed and premedicated with a 1.0 mg/kg subcutaneous injection of buprenorphine (SR-LAB; Zoopharm, Windsor, CO), and then anesthetized with inhaled isoflurane (2–3.5%:95% isoflurane:oxygen mixture) delivered via nosecone. The dorsum of the head from the intercanthal area to the cranial cervical region was clipped and prepared for aseptic surgery. Anesthetized rats were placed in a small animal stereotactic headframe (Model 1350M, David Kopf Instruments, Tungisten, CA). A unilateral rostrotentorial surgical approach to the skull was performed and a 3 mm in diameter parietal craniectomy burr hole defect was created in the skull of each rodent using a high-speed electric drill. Randomly selected, sterile fragments of FMD (2-5 mm length; outer diameter = 365 μm; inner diameter = 150 μm) made from fused-silica capillary fibers (Figure 1 inset; TSP180375, General Separation Technologies, Newark, DE) were inserted

through the burr hole, and implanted such that each fragment was completely embedded in the neuropil.[12] Following FMD implantation or sham treatment, the surgical incision was closed with tissue adhesive (VetBond, 3M Animal Care Products, St. Paul, MN).

Animal Health Status Monitoring and Euthanasia

Rats were housed in a temperature (26 +/-1.5°C) and humidity controlled experimental room with a 12h:12h light-dark cycle in transparent polycarbonate cages, with 2 rats in each cage. Laboratory chow and water were provided ad libitum throughout the experiment. Rats underwent a 14 days acclimation period prior to the performance of the sham or FMD implantation surgery on day 0.

After craniectomy procedures, a health check was performed each day for the 180 days period of the study to examine signs of lassitude, social withdrawal, locomotion incoordination, dehydration, and surgical wound dehiscence or infection. The body weight of each animal was also recorded on the day of each of the predetermined survival endpoints, and animals were euthanized by intraperitoneal barbiturate overdosage (30 mg/kg Fatal Plus, Vortech Pharmaceuticals, Dearborn, MI).

Hematological and biochemical analysis

For each rat, prior to the euthanasia, blood was collected via an intracardiac puncture and aliquoted into EDTA anti-coagulant and serum separator vacutainer tubes. Hemoglobin (Hb; %), hematocrit (Hct; %), mean corpuscular volume (MCV; fL), mean corpuscular hemoglobin (MCH; pg), red blood cell count (RBC; $\times 10^6/\mu L$), total white blood cell count (WBC; $\times 10^3/\mu L$), lymphocytes (%), monocytes (%), granulocytes (%) and platelets ($\times 10^3/\mu L$) were determined using Sysmex XT-2000i analyzer (Sysmex, Mundelein, IL). Serum alanine transaminase (ALT; U/L), aspartate transaminase (AST; U/L), alkaline phosphatase (ALP; U/L), total bilirubin (mg/dL), albumin (g/dL), total protein (g/dL), cholesterol (mg/dL), glucose (mg/dL), blood urea nitrogen (mg/dL), and creatinine (mg/dL) were determined in serum with an AU400 analyzer (Olympus America, Center Valley, PA).

Micro-Computed Tomographic (mCT) Imaging

Following euthanasia, each rat was decapitated and a mCT scan of the head obtained (IVIS Spectrum CT, Perkin Elmer Caliper Life Sciences, Waltham, MA) using the following acquisition parameters: voxel size= 75μm, 50 kV, 1mA, FOV: 6x6x3 cm to document the location of the FMD fragment in the brain. Decapitation was necessary because the mCT unit was designed to accommodate mice, and it was not possible to the fit the body of an adult rat in the mCT gantry.

Necropsy, Histopathology, and Immunohistochemistry

Following euthanasia and mCT, a necropsy examination was performed on each rat. Following immersion fixation in 10% neutral buffered formalin for 24 hours, the extracted brain of each rat was mounted into a 2mm matrix slicer (Zivic Instruments, Pittsburg, PA) and sectioned in the transverse plane. Paraffin embedded tissues were sectioned at 5μm and stained routinely with hematoxylin and eosin (H&E, Abcam, Cambridge, MA). Histological slides of the brain stained with H&E were scored using a modification of previously reported grading system that accounts for brain and meningeal tissues responses to the presence of catheters in the nervous system (Supplemental Table S1).[16] Additional paraffin embedded, 3 μm brain sections were stained according to the manufacturer's instructions with primary antisera against glial fibrillary acidic protein (GFAP; polyclonal, 1:150, Dako, Carpinteria, CA), with an alkaline phosphatase detection method and fast red counterstain.

Statistical Analyses

At each time point, unpaired t-tests were used to compare means of body weight, hematologic and biochemical variables, and histologic scores between sham control and FMD implanted groups, with significance defined as $p < 0.05$. All data were analyzed using Prism 9 software (version 9.2.0, GraphPad Software, San Diego, CA).

RESULTS

Animal Health Status

Clinical abnormalities were not observed in 14/16 sham controls or in 15/16 FMD implanted rats. Two sham control animals experienced surgical wound dehiscence in the first three days post-operatively, which were treated with primary wound closures with suture and subsequently resolved. One FMD implanted rat in the 180 days survival group developed a 5 mm in diameter, palpable subcutaneous soft-tissue swelling overlying the surgical site 126 days after the surgery, but this was not associated with other alteration in behavior. At the 180 days survival endpoint, this palpable swelling had increased in size to ~10 mm diameter. No differences in body weight (Figure 2) were noted between sham control or FMD implanted rats.

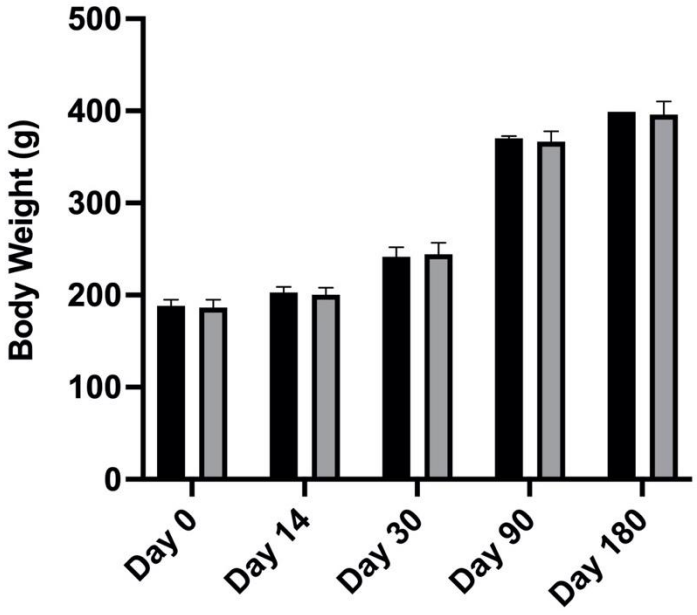

Figure 3-2. Mean body weights of sham control (black) and FMD implanted rats (grey) groups over the study period.

Hematologic and biochemical analysis

No differences in any hematologic or biochemical variables were observed between sham control and FMD implanted groups at any time point in the study (Table 1).

mCT Imaging

Well marginated craniectomy defects were clearly visible in all sham controls and 15/16 FMD implanted animals (Figure 3). No imaging abnormalities within the brain were observed on mCT of any sham control rats. In 16/16 FMD implanted rats, the FMD fragment was visible on mCT as an intact well demarcated, linear hyperattenuating object within the brain parenchyma in the location and trajectory of original implantation relative to the overlying craniectomy defect (Figures 3B and 3C, arrows). No evidence of intracranial hemorrhage, air, or other brain lesions were observed on the mCT scans of treated rats. In the one FMD implanted rat in the 180 days survival group (rat 17) with the palpable cranial swelling (Figures 3E and 3F, asterisk), soft tissue swelling and mineralization were observed on mCT in the area of the palpable swelling as well as expansile region of bone lysis associated with the craniectomy defect.

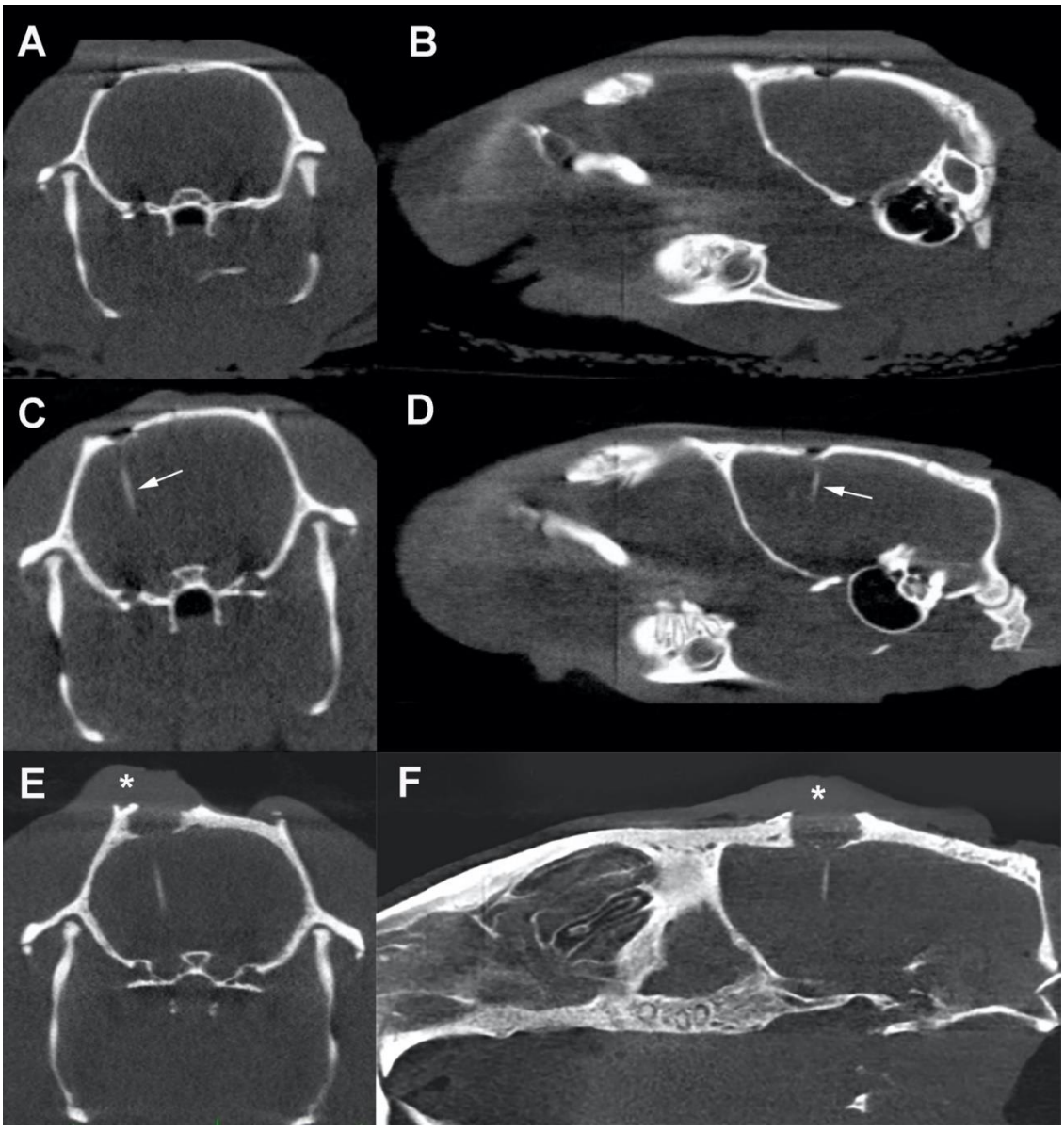

Figure 3-3. Representative micro-computed tomographic scans of control (A, B) and FMD implanted (C-F) rats, and from the one FMD implanted rat that developed a surgical site pyogranuloma and calvarial osteomyelitis (E, F)

Representative micro-computed tomographic scans of control (A, B) and FMD implanted (C-F) rats obtained at day 90, and from the one FMD implanted rat that developed a surgical site pyogranuloma and calvarial osteomyelitis (E, F) 180 days after treatment.

The implanted FMD are visible as linear, hyperattenuating objects (arrows) within the brain parenchyma underlying the craniectomy defects. The soft tissue swelling (E, F asterisk) and expansile, osteolytic reaction in rat 17 are apparent.

Necropsy, Histopathology, and Immunohistochemistry

No gross lesions were observed in the brains of sham controls (Figure 4A1). On gross examination of FMD implanted rats, focal meningeal exudates were observed on the dorsal surface of the cerebrum and were visible at the point where FMD fragments were inserted into brain in the day 14 and 30 (Figure 4A2) groups. In the day 30 and 90 groups, punctate depressions on the dorsal aspect of the cerebrum were observed where FMD fragments were inserted into the brain. In some animals, the brain extraction procedure resulted in the proximal tip of the FMD fragment protruding into the center of these depressions (Figure 4A3). Following transverse sectioning of the brain, implanted FMD fragments were clearly visible, but were not associated with grossly apparent lesions in the brain parenchyma (Figure 4A4). FMD implanted rat 17 was the only animal with an observable gross lesion outside of the brain. This rat had a palpable soft-tissue swelling on the head, was noted to have an epidural abscess affecting the calvarium immediately adjacent to the craniectomy site extending into the overlying soft tissues.

Histological scores in FMD implanted rats were significantly higher than controls at days 30 and 90 (Figure 4B). The severity of histologic lesions successively increased in both sham and FMD implanted groups over days 14-90 of the study, with very mild lesions present in sham control and FMD implanted rats by study day 180.

In sham controls, histologic lesions consisted of surface contusions and mild hemorrhage, edema, and mixed suppurative and mononuclear brain parenchymal and meningeal inflammatory infiltrates that were localized to catheter tracks or the craniectomy site on Day 14 (Figures 4C1 and 4C4). On days 30 and 90, inflammatory infiltrates in the meninges and brain were predominantly mononuclear and contained hemosiderin laden macrophages (Figure 4C7). Increased numbers and sizes of glial cells, which were confirmed to be predominantly astrocytes on GFAP immunohistochemistry, were noted

adjacent to catheter tracks (Figure 4C4). Sham control animals had minimal lesions consisting of scant gliosis along the catheter insertion tracks at day 180 (Figure 4C10).

In FMD treated rats, observed meningeal infiltrates were similar in type but slightly more extensive than those observed in controls (Figures 4C2, 4C3, and 4C5) at the same time points. Brain parenchymal edema, inflammation, astrogliosis, and hemorrhage were also similar in morphology to controls but more severe in their regional extent of involvement of the brain surrounding the FMD implants (Figures 4C2, 4C5, and 4C6). Brain parenchymal necrosis localized to distal tips of the FMD was also observed in treated rats at days 30 (Figure 4C5) and 90 (Figures 4C8 and 4C9). The predominant histological brain lesion in the day 180 FMD group was mild gliosis along the catheter implant tracks (Figure 4C11, arrow). In the day 180 FMD implanted rats, one animal (rat 17) had a pyogranulomatous epidural mass, meningeal fibrosis, and calvarial osteomyelitis in the region of the craniectomy. Angular, refringent polarizing material was detected within the pyogranuloma, consistent with silica glass fragments (Figure 4C12). Histologic changes were not observed in the brain parenchyma of rat 17.

Localized astrogliotic reactions, as evaluated with GFAP immunohistochemistry, adjacent to catheter tracks and catheter tips were noted in all groups at all time points. These were interpreted as minimal in the day 14 groups, mild in both 30 days groups, and subsequently decreased in severity at 90 and 180 days, with the extent of reaction in the 180 days groups resembling those seen in the day 14 groups (Figure 4D). Astrogliotic reactions in FMD implanted rats resembled those of control rats in morphology, but extended further into the brain parenchyma surrounding the FMD implants.

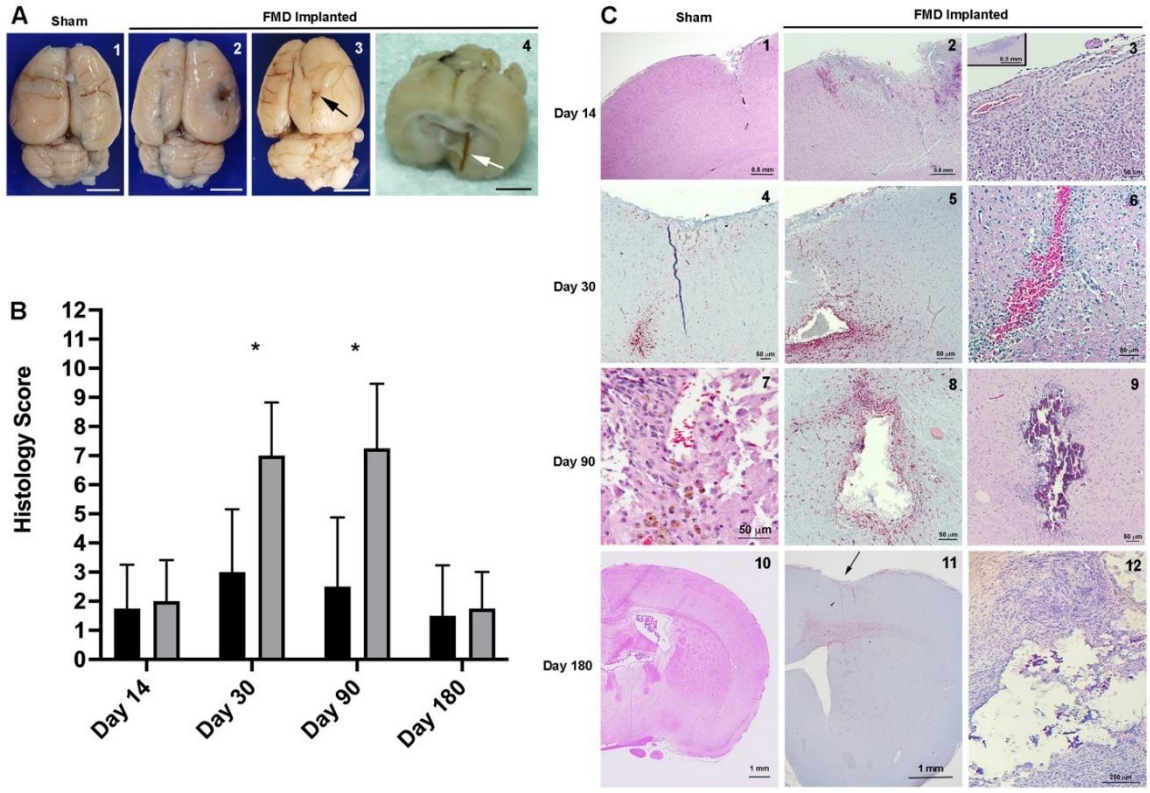

Figure 3-4. Summary of neuropathological findings. A- Gross brain specimens were unremarkable in sham controls (1, day 14). In FMD implanted rats, focal meningeal exudates were visible on the brain surface at the implantation site on days 14 and 30 (2) in FMD implanted rats, and punctate depressions in the brain were seen at the implant site (3, day 90, arrow). FMD fragments were clearly visualized within the brain tissue upon sectioning, but were not associated with gross lesions (4, day 180, arrow). Bar = 3mm in all panels. B- FMD implanted rats had significantly higher histologic scores than controls at days 30 (*, p = 0.03) and 90 (*, p=0.02). C- Focal meningeal and brain parenchymal inflammatory infiltrates (1-7) and astrogliosis (4, 5, 8) are present surrounding the implantation site at days 14-90 and are more extensive in FMD implanted animals than controls. Brain necrosis at catheter tips (5, 8, 9) was visible in day 30 and 90 FMD implanted rats. Lesions were minimal in day 180 groups, and consisted of mild gliosis along the catheter track (10, 11, arrow). Angular, refractile silica fragments are visible among the pyogranulomatous reaction (12) observed in rat 17 at day 180. Panels 1-3, 6, 7, 9, 10, and 12, H&E stain. Panels 4, 5, 8, 11, GFAP immunohistochemistry.

DISCUSSION

As the CETCS system was originally intended for single use, short duration interstitial delivery of infusates into the brain, this study was primarily conducted to evaluate the biological responses to mechanical device failure.[11] However, given the advantages the photothermal capabilities of the FMD, we also envision the potential value of chronically implanting the device in the brain for long-term continuous or intermittent infusions or optogenetic therapies for neurodegenerative disorders.[17]

In rats with FMD chronically implanted in the brain, we did not observe evidence of neurologic or systemic constitutional illness, hematologic or biochemical abnormalities, or migration of the devices outside of the calvarium. The tissue reactions in the brain associated with the FMD consisted of hemorrhage, inflammation, and astrogliosis at the implant site, and were more locally robust than seen in controls.

Silica based medical devices and biomaterials have been developed and used for over 6 decades for numerous indications, but the major current medical use of silica implants is for bioactive glass applications in bone healing, although fused silica and ceramic catheters have been used for CED applications in the brain.[4,6,19,20] The brain tissue responses we observed to the fused silica FMD fragments were similar in morphology, extent, and temporal evolution to other studies that have reported brain pathology associated with implanted catheters made of silica and other biomaterials.[6,16,20-22] In our study, the mechanical damage to the brain tissue and resulting inflammation were restricted to the implant sites, with the most severe lesions occurring around the tips of the devices, and these injury responses declined in severity between 3 and 6 months.[16] A biocompatibility study of silicon oxide coated nanowires implanted in the rat brain evaluated local effects of the nanowires at 1, 6 and 12 weeks after implantation, and also observed increased glial responses in the first week, which declined over time.[21] This study also found evidence that the nanowires were able to cross the blood brain barrier and leave the brain, and were partially degraded by microglia by weeks 6 and 12.[21]

The FMD device can be clearly visualized with computed tomographic imaging, which is important to confirm its intended location for clinical indications in the brain, but also to monitor catheter placement and integrity when chronically implanted. Although we did not see any signs of distant FMD migration, this is likely because the size of the implanted fragment was too large to pass intact through the rat brain vessels. However, given the clinical, mCT, and histologic findings observed in the one FMD treated rodent in the 180 days survival group, we suspect that the proximal end of the FMD migrated locally through the meninges into the overlying soft-tissues and was damaged. The subsequent mechanical irritation and presence of the silica fragments subsequently led to the pyogranuloma and osteomyelitis at the surgical site, which is a clinical situation that clinically could have been mitigated with a relatively straightforward local debridement intervention. Given the robust and mixed osteoproductive and osteolytic bone tissue response observed in the skull of this rat, we cannot completely exclude the possibility that the fused-silica FMD device has bioactive glass properties upon degradation.[18]

We have used both FMD and the CETCS system to perform CED and laser interstitial thermotherapy in the brain of multiple animal model systems without evidence of mechanical device failure.[10-12,23] However, the observations in the rat with the pyogranuloma highlights the need to evaluate other modes of mechanical failure of the FMD device that simulate the presence and degradation profiles of pulverized silica microfragments within tissues over a more protracted period. This design scenario would be appropriate to model biological and clinical effects of systemic biomaterial migration and intravascular object embolization.

CONCLUSIONS

Chronically implanted FMD fragments in the rat brain were well tolerated clinically, did not migrate distantly or cause significant systemic alterations, and resulted in anticipated mild, localized brain tissue responses that diminished in magnitude over the 6 months study period and were comparable with other implanted biomaterials in the brain. From this biocompatibility data and our clinical experience, we conclude that the risk-benefit profile

of the CETCS device is favorable given its primary intended indication for single, short-term use in the treatment of malignant glioma.

Acknowledgements

This study funded by National Institutes of Health, grant number is NIH/NCI P01207206

REFERENCES

1. Raghavan, R., et al., *Convection-enhanced delivery of therapeutics for brain disease, and its optimization.* Neurosurg Focus, 2006. 20(4): p. E12.

2. Rossmeisl, J., *Maximizing Local Access to Therapeutic Deliveries in Glioblastoma. Part V: Clinically Relevant Model for Testing New Therapeutic Approaches*, in *Glioblastoma*, S. De Vleeschouwer, Editor. 2017: Brisbane (AU).

3. Krauze, M.T., et al., *Reflux-free cannula for convection-enhanced high-speed delivery of therapeutic agents.* J Neurosurg, 2005. 103(5): p. 923-29.

4. Ung, T.H., et al., *Convection-enhanced delivery for glioblastoma: targeted delivery*
of antitumor therapeutics. CNS Oncol, 2015. 4(4): p. 225-34.

5. Vogelbaum, M.A. and M.K. Aghi, *Convection-enhanced delivery for the treatment*
of glioblastoma. Neuro Oncol, 2015. 17 Suppl 2: p. ii3-ii8.

6. Rossmeisl, J.H., et al., *Phase I trial of convection-enhanced delivery of IL13RA2 and EPHA2 receptor targeted cytotoxins in dogs with spontaneous intracranial gliomas.* Neuro Oncol, 2021. 23(3): p. 422-34.

7. Mehta, A.M., A.M. Sonabend, and J.N. Bruce, *Convection-Enhanced Delivery.* Neurotherapeutics, 2017. 14(2): p. 358-71.

8. Sampson, J.H., et al., *Poor drug distribution as a possible explanation for the results of the PRECISE trial.* J Neurosurg, 2010. 113(2): p. 301-9.

9. Vogelbaum, M.A., et al., *First-in-human evaluation of the Cleveland Multiport Catheter for convection-enhanced delivery of topotecan in recurrent high-grade glioma: results of pilot trial 1.* J Neurosurg, 2018: p. 1-10.

10. Elenes, E.Y., et al., *Convection-Enhanced Arborizing Catheter System Improves Local/Regional Delivery of Infusates Versus a Single-Port Catheter in Ex Vivo Porcine Brain Tissue.* Journal of Engineering and Science in Medical Diagnostics and Therapy, 2021. 4(1).

11. Hood, R.L., et al., *Fiberoptic microneedle device facilitates volumetric infusate dispersion during convection-enhanced delivery in the brain.* Lasers Surg Med, 2013. 45(7): p. 418-26.

12. Hood, R.L., et al., *Intracranial hyperthermia through local photothermal heating with a fiberoptic microneedle device.* Lasers Surg Med, 2013. 45(3): p. 167-74.

13. Liu, Y., et al., *Ultrasound-Induced hyperthermia increases cellular uptake and cytotoxicity of P-glycoprotein substrates in multi-drug resistant cells.* Pharm Res, 2001. 18(9): p. 1255-61.

14. Saad, A.H. and G.M. Hahn, *Ultrasound-enhanced effects of adriamycin against murine tumors.* Ultrasound Med Biol, 1992. 18(8): p. 715-23.

15. Denton, K.J., et al., *Secondary tumour deposits in needle biopsy tracks: an underestimated risk?* J Clin Pathol, 1990. 43(1): p. 83.

16. Butt, M.T., *Morphologic changes associated with intrathecal catheters for direct delivery to the central nervous system in preclinical studies.* Toxicol Pathol, 2011. 39: p. 213-19.

17. Montagni, E., et al., *Optogenetics in brain research: From a strategy to investigate physiologic function to a therapeutic tool.* Photonics, 2019. 6: p. 92.

18. Henstock, J.R., L.T. Canham, and S.I. Anderson, *Silicon: the evolution of its use in biomaterials.* Acta Biomater, 2015. 11: p. 17-26.

19. Barua, N.U., et al., *Robot-guided convection-enhanced delivery of carboplatin for advanced brainstem glioma.* Acta Neurochir, 2013. 155: p. 1459-65.

20. Hayn, L., L. Deppermann, and M. Koch, *Reduction of the foreign body response and neuroprotection by apyrase and minocycline in chronic cannula implantation in the rat brain.* Clin Exp Pharmacol Physiol, 2017. 44(2): p. 313-323.

21. Eriksson Linsmeier, C., et al., *Nanowire Biocompatibility in the Brain - Looking for*

a Needle in a 3D Stack. Nano Letters, 2009. 9(12): p. 4184-90.

22. Zhong, Y., and R.V. Bellamkonda, *Biomaterials for the central nervous system.* 2008, 5: p. 957-75.

23. Sharma, P., *Multireceptor targeting of glioblastoma*. Neurooncol Adv, 2020. 2: vdaa107

Table 3-1. Hematologic and serum biochemical profiles by group and time

	Group1 (Day 14)				Group 2 (Day 30)				Group 3 (Day 90)				Group 4 (Day 180)			
	Sham		FMD Implant		Sham		FMD Implant		Sham		FMD Implant		Sham		FMD Implant	
Clinicopathologic Parameter	Mean	SD	Mean	SD	Mean	SD	Mean	SD	Mean	SD	Mean	SD	Mean	SD	Mean	SD
Hemoglobin (mg/dl)	15.61	0.78	15.05	0.39	15.09	0.81	15.33	0.41	15.65	0.89	15.4	0.45	15.41	0.32	15.25	0.37
Hematocrit (Hct; %)	50.58	1.16	49.8	0.96	49.02	1.22	50.7	0.98	48.99	1.11	50.95	1.18	50.93	1.04	50.25	1.12
Mean Corpuscular Volume (MCV;fl)	61.19	1.06	61.42	1.29	61.25	0.51	61.07	0.79	61.88	0.39	61.33	0.46	61.5	0.78	61.21	1.02
Mean Corpuscular Hemoglobin (MCH; pg)	19.89	0.35	19.95	0.41	19.65	0.42	19.98	0.51	19.47	0.58	19.9	0.49	19.87	0.46	20.08	0.17
Red Blood Cells ($\times 10^6/\mu L$)	8.04	0.18	7.96	0.15	7.94	0.21	8	0.17	7.92	0.24	7.98	0.14	8.03	0.22	8.06	0.13
Total WBC ($\times 10^6/\mu L$)	8.15	0.84	8.66	0.29	7.93	1.23	8.34	0.7	8.11	0.92	8.55	0.8	7.87	0.83	9.77	3.14
Lymphocytes %	76.8	2.49	75.25	1.49	74.83	2.29	76.23	1.53	74.84	2.23	76.5	0.82	76.29	2.36	69.8	11.8
Monocytes %	3.08	0.26	3.15	0.21	3.18	0.14	3.33	0.33	3.21	0.17	3.15	0.25	3.01	0.13	3.19	0.21
Granulocytes%	18.31	1.12	19.85	0.79	17.58	1.74	18.83	0.64	18.29	1.08	19.9	1.33	18.51	2.02	26.3	12.08
Platelets ($\times 10^3/\mu L$)	783.53	31.67	772.75	28.65	777.84	26.82	793.5	19.64	781.06	32.66	799	29.94	763.56	38.93	775.75	21.31
Alanine Transaminase (ALT; U/L)	43.44	4.27	40.91	6.78	42.97	3.34	41.17	3.76	46.88	5.9	42.14	3.56	44.47	4.93	42.29	3.45
Aspartate Transaminase (AST; U/L)	132.87	9.95	138.46	5.74	143.23	10.48	138.62	8.53	146.61	11.17	141.19	6.96	126.85	13.92	138.26	3.58
Alkaline Phosphatase (ALP; U/L)	369.34	26.29	376.41	9.86	379.37	16.5	388.94	12.17	394.39	24.45	387.86	20.93	359.22	23.78	374.09	65.42
Total Bilirubin (mg/dl)	0.06	0.04	0.07	0.02	0.08	0.03	0.08	0.04	0.07	0.04	0.09	0.03	0.07	0.02	0.08	0.04
Albumin (g/dl)	3.91	0.24	3.95	0.13	3.96	0.21	3.85	0.19	3.94	0.2	4.03	0.22	3.83	0.21	3.93	0.28

Total Protein (g/dl)	6.27	0.29	6.15	0.21	6.28	0.22	6.35	0.13	6.19	0.32	6	0.18	6.37	0.24	6.18	0.19
Cholesterol (mg/dl)	74.26	11.61	72.64	7.14	74.85	9.39	71.06	7.75	69.58	12.13	73.35	10.94	74.62	8.49	77.13	6.76
Glucose (mg/dl)	79.27	8.66	81.75	5.32	84.36	7.57	80	5.6	81.63	6.61	82.25	4.65	70.46	9.83	79.5	7.55
Blood urea nitrogen (mg/dl)	15.21	2.46	16.03	1.63	16.77	3.06	18.25	2.22	18.38	3.25	16.56	2.38	16.17	1.59	15.04	1.41
Creatinine (mg/dl)	0.34	0.06	0.35	0.03	0.33	0.04	0.35	0.05	0.33	0.06	0.36	0.04	0.31	0.06	0.36	0.05

Supplemental Materials

Table S1- Histological grading system for evaluation of brain pathology in response to fiberoptic microneedle device implantation[16]

	Brain Tissue Response					
Severity	**Absent** → **Severe**					
Response Grade	**0**	**1**	**2**	**3**	**4**	**5**
Mechanical Lesion		Surface contact or contusion	Needle track	Surface contact/contusion and needle track	Puncuture of ventricle	Surface contact/contusion, needle track, and puncture of ventricle
Hemorrhage		Mild, focal	Mild, local to	Regional, around needle track	Moderate	Severe

	No lesion		needle track			
Inflammation/ Edema		None	Mild, local to needle track	Regional, around needle track	Moderate	Severe
Parenchymal Necrosis		Absent	Absent		Localized to needle tip	Regional necrosis around and remote from needle tip
	Meningeal Reaction					
Response Grade	**0**	**1**	**2**	**3**	**4**	**5**
Meningeal inflammatory infiltrate	No lesion	Local, mild	Local, moderae	Local, severe	Regional	Diffuse

The total histologic score = Brain tissue response grade + meningeal reaction grade

CHAPTER 4. GLUTAMATE CONCENTRATIONS IN RAT HEALTHY BRAIN AND F98 ORTHOTOPIC GLIOMA MODELS AFTER HIGH FREQUENCY IRREVERSIBLE ELECTROPORATION THERAPIES.

INTRODUCTION

Glutamate is the most abundant amino acid neurotransmitter in the brain (10000-12000 μmol/L), but its concentration in extracellular fluids is very low (0.5-2 μmol/L). Glutamate concentrations in plasma are 50-100 μmol/L [1]. This gradient is particularly important to maintain because excess glutamate in the extracellular fluid lead to overactivation of glutamate receptors which can initiate a number of deleterious consequences in a process called "excitotoxicity", including impairment of calcium buffering, generation of free radicals, and activation of the mitochondrial permeability transition, which ultimately results in cell death [2]. Studies have implicated excitotoxicity as a common pathophysiologic mechanism of disease in a variety of neuropathological conditions such as stroke, traumatic brain injury, neurodegenerative diseases, and glioblastoma GBM [1-3]. Excitotoxicity also promotes brain tumor growth, as extracellular glutamate levels in glioma were found to be 100 times higher than in healthy brain [4, 5], which lead to proliferation and invasion of glioma cells [6, 7]. Not only does glutamate directly cause cell death through perturbations in Ca^{2+} homeostasis, but glutamate also interacts with AKT to promote glioblastoma progression and tumor necrosis. In addition, various cell signaling molecules in the glioma microenvironment, including TNFα, AEG-1, and NF-κB, cause coordinated accumulation of glutamate through reuptake inhibition to promote local excitotoxicity and necrosis [8].

Under normal conditions, the cellular components of Blood Brain Barrier (BBB) regulate the concentration of glutamate in the brain. Astrocytes and brain microvascular endothelial cells express the Na+ dependent excitatory amino acid transporters, EAAT-1 (SLC1A3) and EAAT-2 (SLC1A2) are mainly localized in the plasma membrane of astrocytes, and EAAT-1, EAAT-2 and EAAT-3 (SLC1A1) are present in the abluminal membrane of

endothelial cells of the brain capillaries [2, 9, 10]. The luminal membrane of the endothelial cells has only facilitative glutamate transporters that allows the release of glutamate from endothelial cells to the blood when the intracellular glutamate concentration becomes greater than plasma concentration [2]. Movement of glutamate from the endothelial cells to brain tissue would be difficult due to the Na+ gradient that exists between extracellular fluid and endothelial cells and the lack of facilitative transporters in the abluminal membrane [11].

The BBB can regulate the glutamate concentration, but glutamate can also influence the permeability of the BBB. Glutamate activation of NMDA receptors in endothelial cells produces a calcium influx that results in nitric oxide (NO) synthesis by the calcium-dependent enzyme nitric oxide synthase [12]. Released NO diffuses into adjacent endothelial cells, where it activates a secondary messenger cascade associated with guanylyl cyclase to generate cyclic guanosine monophosphate (cGMP). Increased intracellular levels of cGMP lead to a signaling cascade that causes BBB opening through rearrangement of tight junction proteins away from cell-cell contact regions [13]. At the molecular level, a transient exposure to extracellular glutamate caused an initial redistribution of occludin, followed by a decrease in expression of this tight junction protein [3]. Some biochemical processes involved in this increase permeability of BBB are occludin phosphorylation, specifically an excessive phosphorylation of the tyrosine residues and a decrease in phosphorylation of the threonine residues. The hyperphosphorylation of tyrosine appears to be regulated by the NMDA receptors. In the other hand, the AMPA/KA receptors were involved in glutamate-mediated hypophosphorylation of threonine residues of occludin [3]

High Frequency Irreversible Electroporation (H-FIRE) is a novel, non-thermal tissue ablation technique developed by our lab. H-FIRE utilizes ultrashort (~0.5-2us) bipolar pulses that do not cause muscle contraction, mitigating the need for neuroparalytic agents during treatment as is required for IRE [14], creates a more electrically homogenous environment, resulting in more uniform ablations [15], and that have an ability to selectively ablate cancer cells at lower electric fields than healthy cells [16]. We have

performed H-FIRE ablative treatment for canine patients with intracranial meningiomas and gliomas [17] and in a rodent F98 orthotopic model of neuroinvasive glioma.

Studies in rodent and canine glioma models performed in our laboratory have shown that H-FIRE pulses can also induce BBB disruption by downregulation and degradation of tight junctional proteins [18]. When applied at lower electrical fields (<600 V/cm) in healthy or diseased brain tissue, H-FIRE can also cause BBB disruption without causing any electrically-induced muscle contractions, or brain tissue damage in the treated regions [19]. Temporal profiling of the duration of H-FIRE induced BBB disruption indicated that BBB permeability was greatest 1 hour after H-FIRE treatment, and then decreased exponentially at 24, 48, 72 hours with BBB recovery occurring by 96 hours [20]. It has been demonstrated in rodent models that transient permeabilization of the BBB with PEF markedly enhances the delivery and pharmacologic effects of normally BBB impermeable chemotherapeutic agents in the brain [21, 22]. Thus, H-FIRE can be exploited to facilitate the delivery of conventional or targeted chemotherapeutics to microscopic tumor infiltrates that extend beyond the gross-tumor margins using both ablative and sub-lethal pulsing protocols.

Given the potential effects glutamate has on cell death, GBM tumorigenesis and the BBB, as well as that the biophysical effects of H-FIRE are mediated by altering cellular permeability through the creation of nanoscale pores in cellular membranes, we are interested in examining the effects of H-FIRE therapies on glutamate metabolism on the brain. ***Our overarching hypothesis is that H-FIRE treatment will increase glutamate in the brain, and glutamatergic excitotoxicity may be a mechanism of HFIRE induced cell death and BBB permeabilization***. Glutamate excitotoxicity following H-FIRE will result from endogenous glutamate release by neurons and decreased glutamate uptake by astrocytes and glutamate transporters. Characterization of glutamate metabolism after H-FIRE is important as it may mechanistically contribute to the intended therapeutic effects of H-FIRE, such as tumor cell death and opening of the BBB, but also may mediate potential adverse effects such as collateral death of healthy neurons or the generation of seizures.

MATERIAL AND METHODS

In vivo experiments

- Animals: Male Fischer rats were used for both healthy brain (n=34) and F98 orthotopic glioma implant experiment (n=24).

- Surgical procedure and H-FIRE treatments: A lateral rostrotentorial surgical approach was made and a 5 mm x 2.5 mm rectangular, parieto-occipital craniectomy defect created in the right aspect of the skull using a high-speed Dremel drill, as described in Lorenzo et al. 2019 [20].

- Tumor implantation: Rat malignant glioma cells (F98 cell line, certified pathogen free (Supporting Documents: Charles River certification:F98 cell line testing CR-RADS), ATCC, Manassas, VA) were implanted in the anesthetized rats using sterile, stereotactic surgery. A total of 5,000 - 15,000 cells in 5 μL phosphate-buffered saline were injected into the striatum of the brain during a period of 5 minutes. After the injection, the needle was kept in place for 2 minutes, and then slowly retracted, in order to prevent the spread of tumor cells. The incision was closed with tissue adhesive or absorbent sutures, dressed with application of 10% povidone iodine salve, and re-opened in preparation for HFIRE combinatorial treatment.

- H-FIRE treatments: Custom, blunt-tipped electrodes were placed into the cerebral cortex using stereotactic coordinates referenced to the location of the rostral electrode. The electrodes measure 0.45 mm in diameter, with 1 mm exposure, and 2-6 mm in edge-to-edge separation distance. This two-electrode configuration generates a non-uniform electric field distribution that depends on the applied voltage and dielectric properties of the tissue. For the purposes of all experiments "Low dose" HFIRE is the dose of energy found sufficient to disrupt the blood-brain barrier (BBBD) and the "High dose" H-FIRE is a dose sufficient to ablate brain/tumor cells. For these experiments, the "Low dose" (BBBD) is100-600V,

pulse width 0.5-10 us, burst duration 20-200 us [20]. And the "High dose" (Ablation dose) is 400-1000V, pulse width 0.5-10 us, burst duration 20-200 us.

- Amino acid neurotransmitter high-performance liquid chromatography (HPLC) assays: Rat brain tissue samples (n=3 tissue samples/group) were collected from the HFIRE BBB disruption experiment (IACUC #16-156) and F98 glioma rodent study (IACUC #19-217) to perform the HPLC for glutamate concentrations. The samples were snap frozen and stored at -80°C, then tissues were removed from the freezer, weighed, and then homogenized with 80 µl of 50 µM EDTA in 400 mM HClO4 solution. The homogenized tissue samples were neutralized with 0.1 M borate buffer (1:10) and centrifuged (14,000 rpm, 30 min, 4 ºC). The supernatant (100 µl) was removed and placed in a microcentrifuge tube for the derivatization. The derivatization procedure was based on a protocol previously described by Clarke et al. (2007) [23]. Briefly, 100 µl of either standard or sample supernatant was added to a solution containing 0.1 M borate buffer (900 µl, pH 9.5), 10 mM potassium cyanide (200 µl) and 6 mM NDA (200 µl). The samples were then vortexed and the reaction proceed for 15 min at ambient temperature in the absence of light. The derivatization product (20 µl) was injected onto the HPLC system. The fluorescence intensity comparison of o-phthalaldehyde (OPA) and naphthalene-2,3-dicarboxaldehyde (NDA) were performed using a Shimadzu RF-5301PC spectrofluorophotometer (Shimadzu, Columbia, MD). The amino acids, GABA and glutamate, were derivatized with either NDA or OPA and the duration and intensity of the fluorescent signal was monitored. To derivatize the amino acids with NDA, 0.7 mL of the amino acid standard (< 1M) was added to working solution containing 0.1 M borate buffer (pH 9.5), 10 mM KCN, and 5 mM NDA.24 The OPA derivatization protocol was based on a method described by Rowley et al [24]. The binary gradient HPLC system was constructed using two Shimadzu LC-20AD HPLC pumps (Shimadzu, Colombia, MD) connected with a mixer, on-line degasser, and high-pressure flow channel selection valve. Mobile phase A consisted of 0.1 M Na2HPO4 in 50 mM of EDTA (pH 5.7; adjusted with 6 M HCl), and mobile phase B consisted of 100% methanol. The excitation and emission

wavelengths for NDA-derivatized amino acids were set to 420 and 480 nm, respectively. Known standards were used to identify and quantify the GABA and glutamate peaks in the HPLC chromatogram. Characteristic retention times for GABA and glutamate were 4.5 and 1.8 min, respectively. The peak areas of GABA and glutamate were integrated with the calibration curve of known standards, and all HPLC assays were performed in duplicate. Concentrations were expressed in μmol/mg protein ± standard error of the mean (SEM).

In vitro experiments

The objective of this set of in vitro experiments is to determine the survival of different cell types that constitute the brain parenchyma and glioma after exposing them to different concentrations of exogenous glutamate, and identify a glutamate threshold concentration that would be a surrogate of excitotoxic cell death for each cell line. We then treated each cell line with different H-FIRE protocols, and measured the endogenous glutamate concentration resulting from treatment to determine whether it could potentially reach our identified excitotoxic threshold. We further evaluated the effects of H-FIRE treatment on brain endothelial cell permeability by exposing brain endothelial cells to supernatant obtained from H-FIRE treated cell lines.

- Cell lines: Rat brain striatum neurons (Catalog #: R-CP-502, Lonza), rat astrocytes (CTX TNA2, ATCC), rat brain microvascular endothelial cells (R840-05A, Millipore Sigma) and F98 glioma cells were cultured individually. Dulbecco's modified Eagle's medium (DMEM)/F12, neurobasal medium, B27 supplement and fetal bovine serum (FBS) were purchased from Thermo Fisher Scientific, Inc. (Gibco; Waltham, MA, USA). Trypsin was purchased from Lonza Bioscience (Walkersville, MD, USA). Penicillin and streptomycin were purchased from Biological Industries (Beit Haemek, Israel). Cell culture plates, flasks and inserts were purchased from Corning, Inc. (Corning, NY, USA).

- Cell survival experiment: MTT Cell proliferation assay (ATCC) was used for the measurements. For each cell line (astrocytes, neurons, F98 glioma, and endothelial

cells), 10.000 cells/well were seeded per onto a 96 wells plate, incubated at 37 °C in 5% CO2 in a humidified incubator overnight. Then, 0.5 µM (control), 5µM, 10µM, 50µM, 100µM, 1000 µM, 25 mM, 50mM, and 100mM of exogenous glutamate was applied to the wells. Survival assay was performed 12h and 24h after treatment.

- Glutamate measurement in supernatant after H-FIRE treatment: Additionally, to measure if there is glutamate release by the different types of cells tested after H-FIRE treatment, we applied an HFIRE BBB disruption protocol and ablation protocol to each individual cell line, extracted the supernatant and measured the glutamate concentration using Glutamate Assay Kit (ab83389, Abcam). We applied H-FIRE treatment in cell suspensions using the protocol of 5-5-5, 100 µs, 100 bursts, and we used different voltages (250V, 500V and 1000V) to see if we observe different glutamate concentration release using BBB disruption protocol or the ablation protocol. The kit shows a linear standard curve up to 200 µM glutamate.

- Endothelial Permeability test: Finally, to test whether the supernatant of the post-H-FIRE cell cultures are able to change the permeability of the endothelial cells, we used the In Vitro Vascular Permeability Assay (Millipore). After H-FIRE treatment was applied to cell lines, we extracted and exposed the endothelial cells to the pooled supernatant, to determine if it is a permeability factor. We used Vascular Endothelial Growth Factor (VEGF) at a concentration of 10 nM as control treatment based on literature [25, 26].

Glutamate Neurotransmitter PCR Superarrays

We performed Glutamate and GABA superarrays in rat brain samples from 2 experiments: 1) BBB disruption experiment described in Lorenzo et. al [20], where we had sham group (n=2), group 1: 1h post treatment (n=4), Group 2: 24h post treatment (n=8), group 3: 48h post treatment (n=8), group 4: 72h post treatment (n=8) and group 5: 96h post treatment (n=4). In the second experiment, we used F98 glioma cells implanted rat model as a control

group (n=5), and 2 different H-FIRE treatments were applied: Ablation protocol (n=7) and BBB disruption protocol (n= 5). The brain tissue was stored in RNA later solution. 500 nanograms of mRNA was reverse transcribed using first strand kit reverse transcriptase (Qiagen) according to manufacturer's instructions and synthesized cDNA were diluted 1:3 with RNA free water. 25 µL of this solution were used for each well in GABA and Glutamate RT2 Profiler PCR Arrays plate (Qiagen). Quantitative real-time PCR was performed on an ABI Fast Block 7500. Samples were run in triplicates and Qiagen Gene Globe tool were used to perform the analysis. The mean Ct value from the triplicate reactions was used for fold-change analysis.

Statistics

Kruskall-Wallis tests were used to compare glutamate concentrations, cell cytotoxicities, and endothelial cell permeability across treatment groups. In cases where the Kruskall-Wallis test showed significance, Dunn's test was used for pairwise comparison between the treatment groups and the sham or control group. In the gene exression experiments, the mean Ct value from the triplicate reactions was used for fold-change analysis.

RESULTS

In vivo experiments

In the healthy rodent brain, the basal glutamate concentration in the sham condition was 93.13 µmol/mg protein, and we observed a significant and serial increase in the glutamate concentration after H-FIRE BBB disruption treatment at each time point from 1-96h post-treatment, reaching the maximum value in the 72h post-treatment (153.24 µmol/mg protein; Figure 4-1A). The glutamate concentration at 10 days post-treatment was not significantly different between shams and treated animals (Figure 4-1A).

When we applied H-FIRE with ablation protocol, we performed glutamate measurements at 24h and 10 days post-treatment, and observed a significant increase in the glutamate concentration at 24h post-treatment (Figure 4-1B).

In the F98 orthotopic glioma rodent model experiment, the glutamate concentration was higher compared to the normal brain conditions. The basal concentration was 130.27 µmol/mg protein, and we observed a significant increase in the 24h post-treatment timepoint both using BBB disruption protocol and ablation protocol (381.27 and 1334.51µmol/mg respectively) (Figure 4-1C and Figure 4-1D). In the measurements made in 10 days post-treatment timepoint evidence that the glutamate levels returned to the basal concentration.

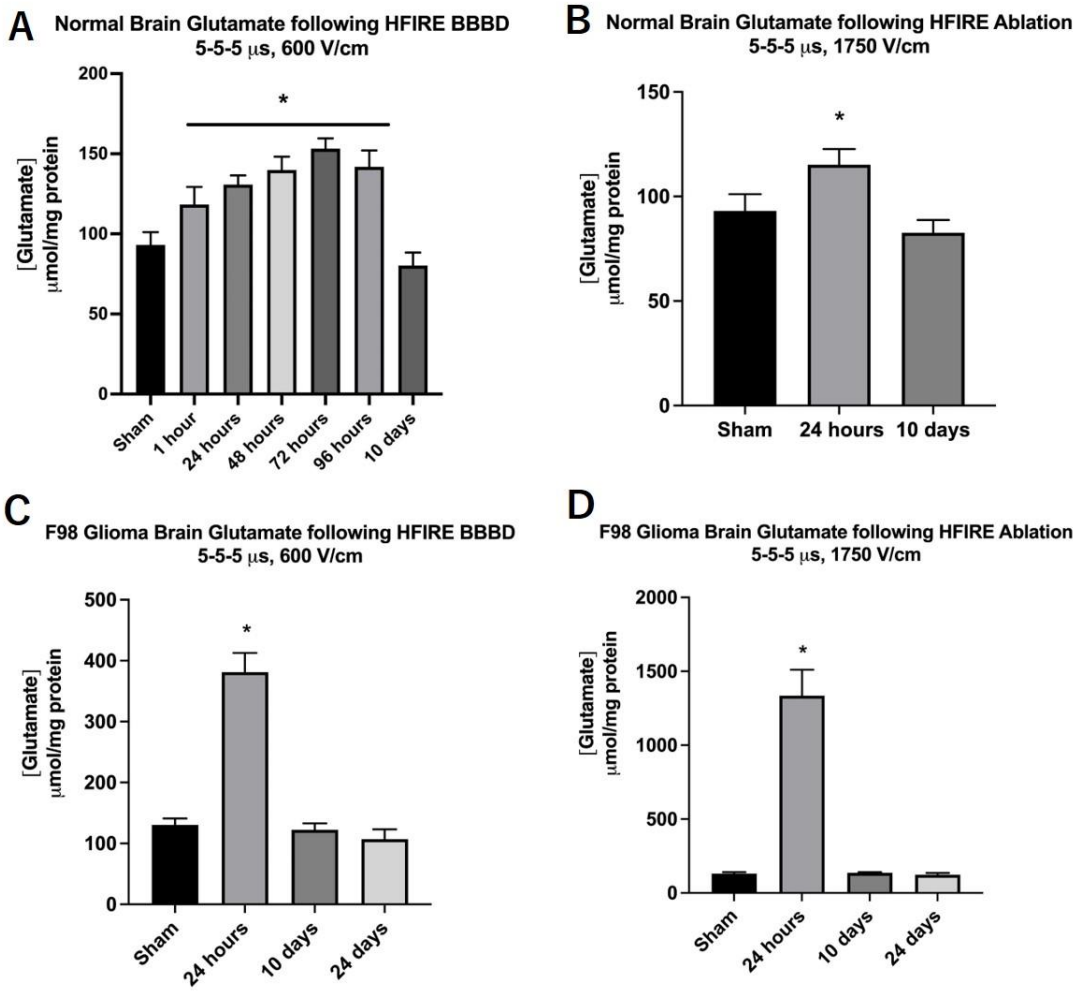

Figure 4-1. Glutamate concentrations measured using HPLC in different experiments

Figure 4-1. Glutamate concentrations measured using HPLC in different experiments. A) healthy rat brain model using H-FIRE BBB disruption protocol and measured in 1h, 24h, 48h, 72h, 96h and 10 days post-treatment timepoints. B) Healthy rat brain model using H-FIRE ablation protocol. C) F98 orthotopic rat model using H-FIRE BBB disruption protocol. D) 98 orthotopic rat model using H-FIRE ablation protocol. An asterisk (*) indicates the value is significantly ($p < 0.05$) different from the sham.

In vitro experiments

Cell survival: Cell viabilities decreased significantly to close to 0% at and above concentrations of 25mM glutamate in all the cell types and in both timepoints (12h and

24h) (Figure 4-2). At 12h post-treatment, viability was significantly decreased in astrocytes and neurons at a glutamate concentration of 10mM, but not in endothelial or glioma cells. At 24h post-treatment, significant decrease in neuronal viability were observed at concentrations of glutamate >5 μM.

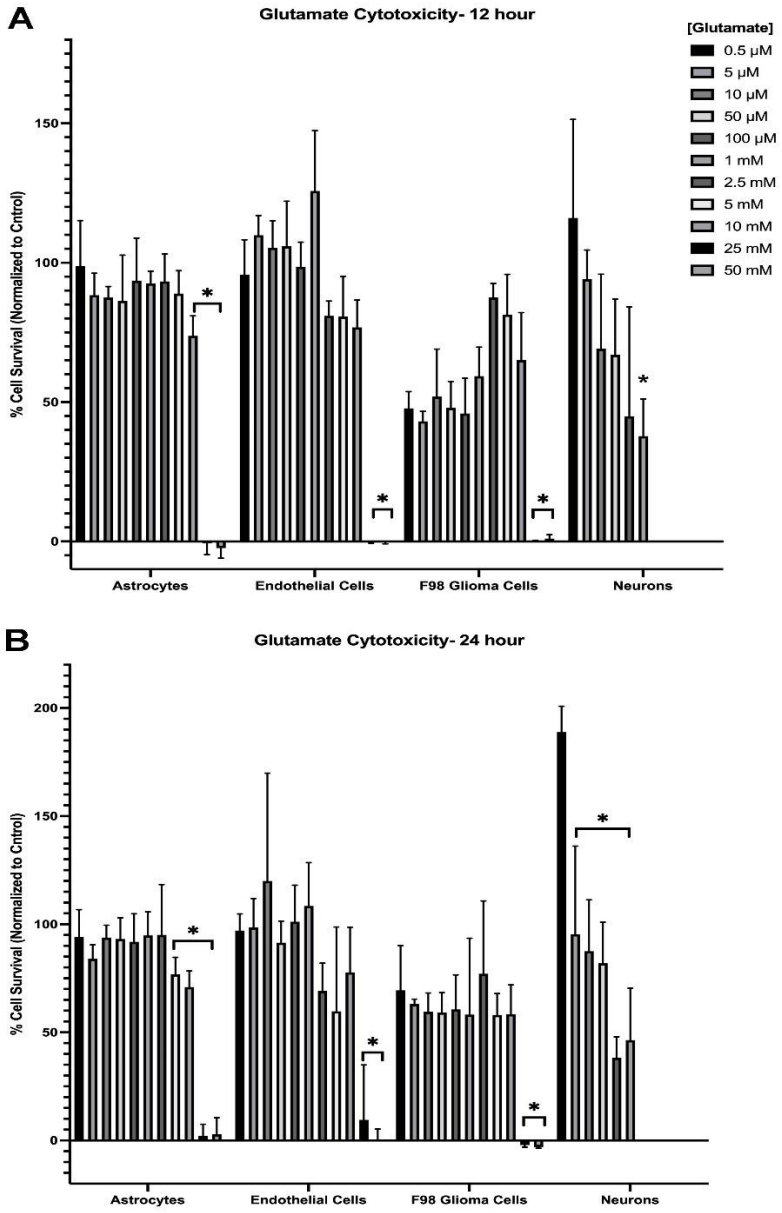

Figure 4-2. Cell survival after application of exogenous glutamate measured post 12h and 24 h in rat cell lines of astrocytes, brain endothelial cells, F98 glioma cells and brain striatum neurons. An asterisk (*) indicates labeled values significantly different ($p<0.05$) than negative controls.

Glutamate concentration after H-FIRE treatments: The measured glutamate increased in the supernatant of all cell limes in all cell lines after H-FIRE treatment, but not all post-treatment increases were statistically significant (Figure 4-3).

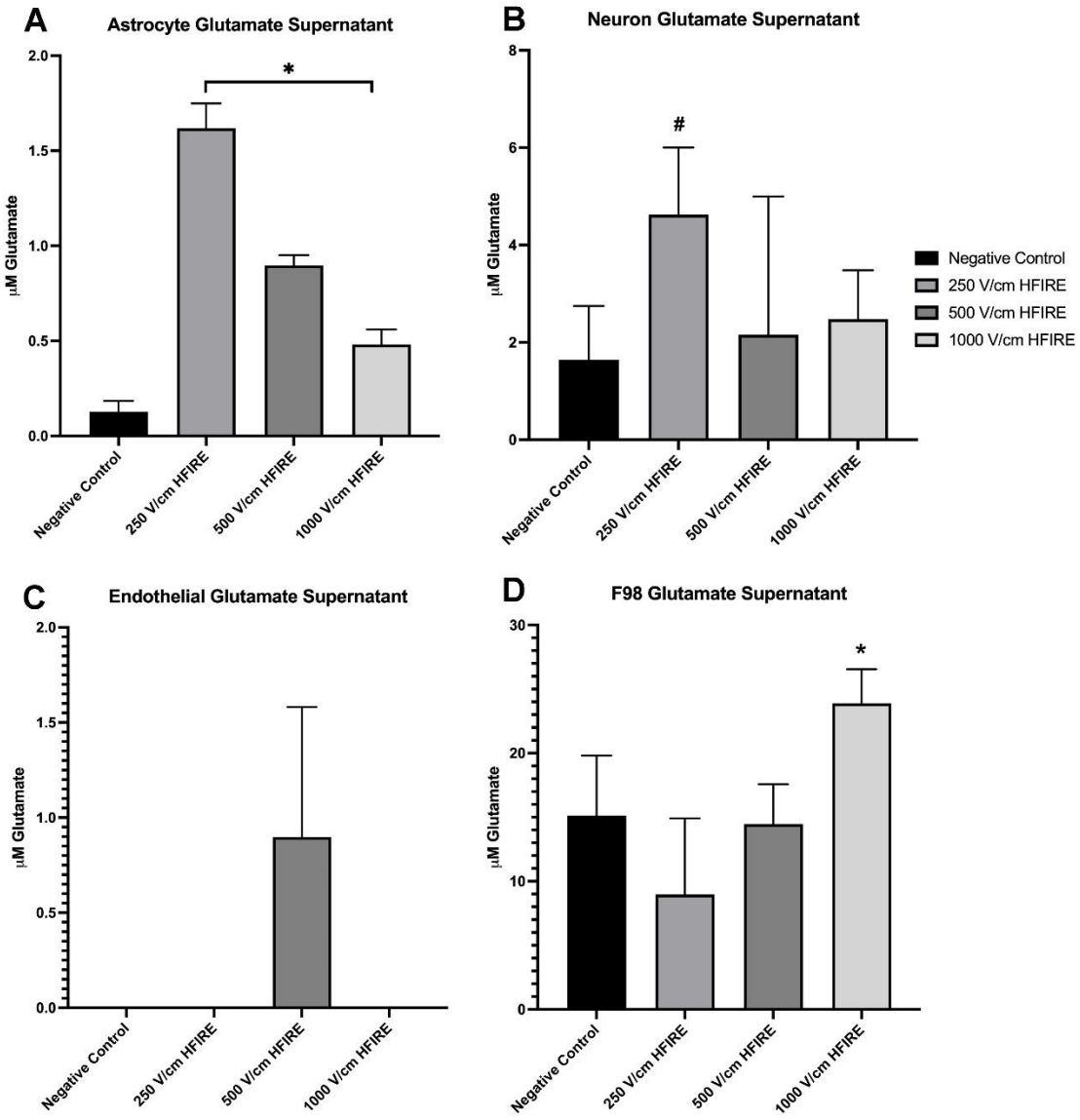

Figure 4-3. Glutamate concentration after H-FIRE treatment in cell cultures

Figure 4-3: Glutamate concentrations measured in the supernatants of H-FIRE treated astrocytes (A), neurons (B), endothelial cells (C), and F98 glioma cells. An asterisk (*) indicates the labeled treatment condition(s) were significantly ($p < 0,05$) different than all other groups. A # indicates the labeled treatment was significantly different from the negative control.

Permeability test in endothelial cells: The permeability of the endothelial monolayer didn't change after we applied the supernatant of the cells after H-FIRE treatment (Figure 4-4).

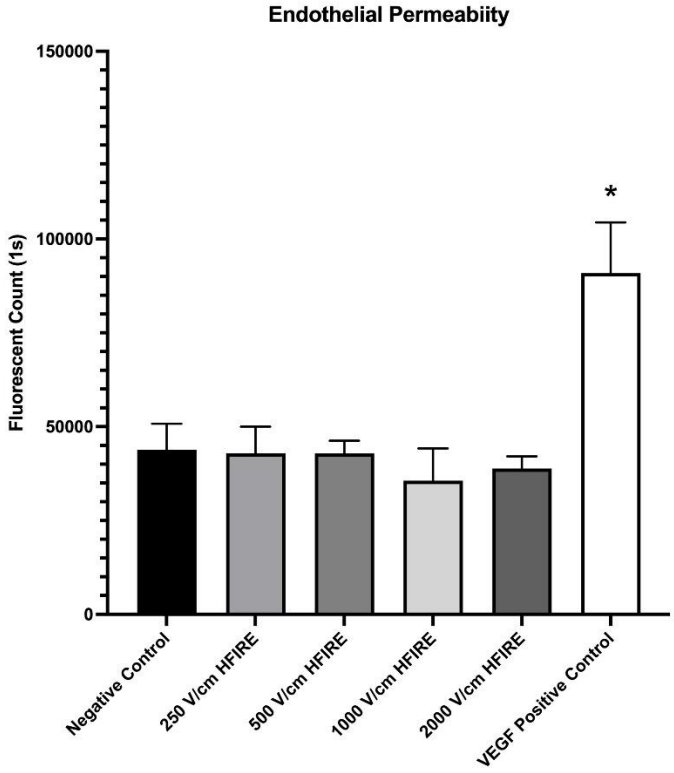

Figure 4-4. Endothelial permeability assay using the supernatant of H-FIRE treated F98 cells. An asterisk (*) indicates labeled value significantly different ($p<0.001$) than negative controls.

Neurotransmitter PCR superarrays

In the BBB disruption study, we found up-regulation of the majority of glutamate receptors genes 96 hours post H-FIRE treatment (Figure 4-5A). Specifically, the ionotropic NMDA receptors (Grin1, Grin2a, Grin2b) have higher fold change compared to other ionotropic receptors in the 96h timepoint group (fold change = 21.51, 27.68 and 14.35 respectively). The principal glutamate transporter that was upregulated in 96-hour timepoint group was EAAT2 (Slc1a2, fold change = 43.90).

In the F98 glioma cell implanted rat model, we found different and distinct clustering of glutamate receptor expression in each group (Figure 4-5B). AMPA receptors (Gria1,

Gria3) and kainate receptors (Grik4) were upregulated in ablation protocol compared to control, in the other hand, NMDA receptors (Grin1, Grin2b, Grin2c) were upregulated in BBB disruption protocol group. Also, the glutamate transporters genes are upregulated in the in the ablation protocol group, specifically the ones for EAAT2 (Slc1a2) and EAAT3 (Slc1a1), normally present in astrocytes for glutamate recycling.

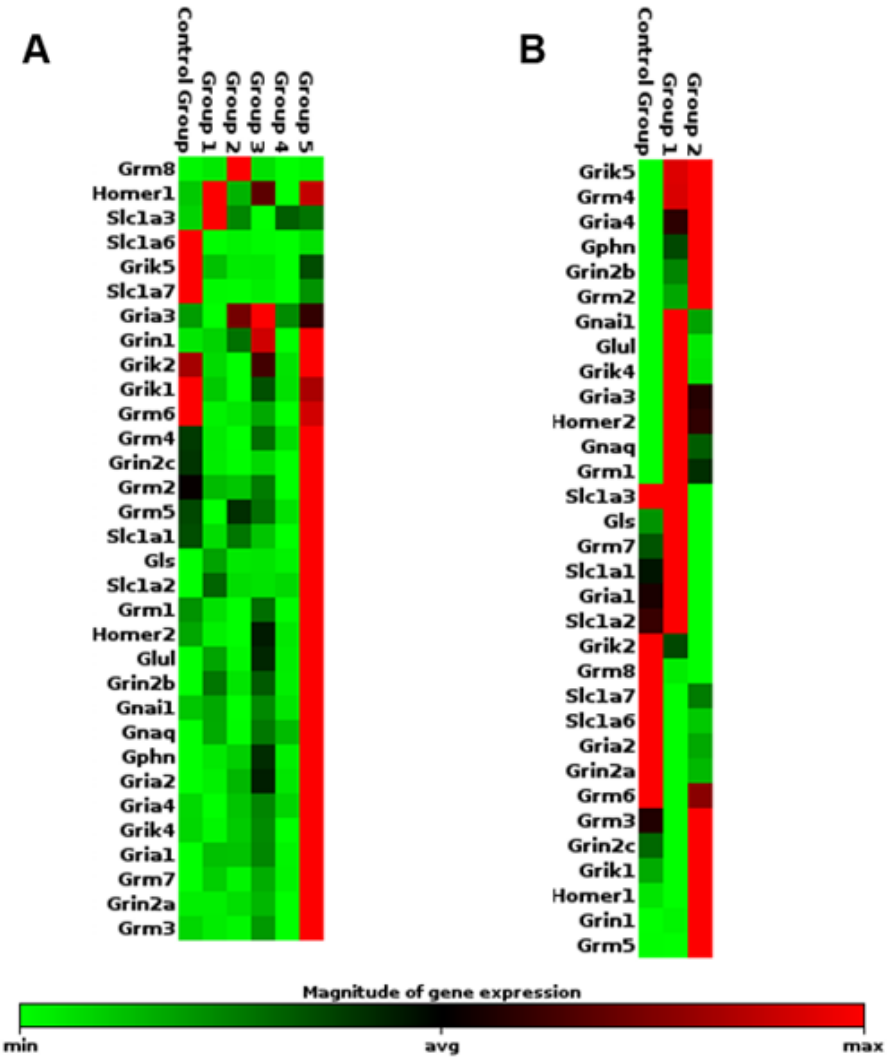

Figure 4-5. Clustergrams for glutamate receptor gene expression

Clustergrams for glutamate receptors gene expression in BBB disruption experiment in normal rat brains (A) described in [1] and in rats implanted with F98 glioma (B). Panel A key: Group 1: 1h post H-FIRE; Group 2: 24h post H-FIRE; Group 3: 48h post H-FIRE; Group 4: 72h post H-FIRE; Group 5: 96h post H-FIRE. Panel B key: Group 1: Ablative dose H-FIRE treatment; Group 2: BBB disruption dose H-FIRE treatment.

DISCUSSION

The baseline in vivo glutamate concentration in rat brain measured by HPLC in the control group obtained in our study was similar of the values described by Zieminska et al. [27]. The effect of the H-FIRE treatment on increasing the glutamate concentration seen in our is possibly related to the permeabilization of the BBB or increasing the permeability of neuronal membranes in the region of treatment, as we observed increased glutamate concentrations after treatment with BBBD and ablative H-FIRE protocols. The contribution of permeabilizing the BBB to the increase in gluatamate in further supported by decline of the glutamate at 96 hours after treatment, which corresponds with the BBB recovery time described by Lorenzo et.al [20]. In that study, the maximum volume of BBBD was observed in the 1h post-treatment timepoint, and the BBB was returned to normal after 96h post-treatment.

Neuroexcitotoxicity due to excessive glutamate has been linked to different pathological states of the central nervous system, both chronic, such as epilepsy, sclerosis and Huntington's, Alzheimer's and Parkinson's diseases [28, 29]. It has also been related to acute conditions such as global and focal hypoxia, ischemia, stroke, brain trauma, and hypoglycemia[30, 31]. A loss of glial glutamate transporters and/or a dysfunction of those has been suggested to be the mechanisms of the phenomenon. Excessive NMDA receptors activation can cause a pathological increase in intracellular calcium, which activates cell death signaling to produce apoptosis. NMDA receptor genes were upregulated in our results, suggesting the activation of glutamate-mediated excitotoxic pathway.

Glutamate concentrations under healthy conditions rarely increase to level associated with excitotoxicty because of the efficient reuptake system and metabolism. The EAAT present in astrocytes are the most important regulation factor, responsible for an estimated of 80-90% of extracellular glutamate uptake in the brain [32]. EAATs are present in other components of the BBB such as neurons and endothelial cells, but their function has less impact compared to astrocytes. The results of our glutamate related gene expression data

show an upregulation of EAAT2 (Slc1a2) following HFIRE treatment, suggesting the role in glutamate uptake by astrocytes in conjunction with BBB recovery following treatment.

In the presence of glioma, the extracellular glutamate levels increase significantly. Gliomas release significant quantities of glutamate into the extracellular space. An in vitro study described that a monolayer of glioma cells maintained in a culture flask achieved glutmate concentrations exceeding 500 μM within 12h [33]. In our study, the basal glutamate concentrations in glioma implanted rats were significantly higher compared to the healthy rats, as described in the literature. Behrens et al (2000) measured the glutamate concentration in the extracellular fluid in the peritumoral area of RG2 glioma cells-implanted Fisher rats. They found that the peritumoral region showed 4-fold elevated glutamate compared to normal brain. The H-FIRE treatment in glioma cells implanted rats of our study caused an initial elevation in glutamate concentration 1-hour post-treatment, with a tendency to normalize to basal levels over time. The glutamate values 10 days post-treatment were not significantly different from the control group. Also, the transient increase of the glutamate concentration is much higher when we used the ablation protocol compared to the BBB disruption protocol. This is possibly explained by the cell mortality in the ablated tumor-brain area in addition of the BBB permeabilization area in the tumor margins.

For the in vitro experiments, authors report a range of concentrations of glutamate that are capable of producing significant cytotoxicity in brain cells. Kutzing et al. (2011) reported that treating the rat cortical cells with 175 and 250 μM glutamate results in a loss of overall activity in the higher concentration [34]. Zhang and Bhavnani (2006) showed that 1 mM of glutamate treatment in rat cortical neurons induced one fold increase (50%) in cell death compared with the control group, and 8 mM of glutamate treatment was necessary to produce the same effect in the HT22 mouse hippocampal cell line [35]. Also, Zhang et al. (2019) reported the protective effect of the astrocytes when they are co-cultured with rat cortical neurons. The neurotoxic half-maximal inhibitory concentration in the absence of astrocytes was 364.5, 258.5 and 138.3 μM in 15, 30 and 60 min timepoint respectively, while in co-culture with astrocytes was 1,935, 932.8 and 789.3 μM, evidencing the

important role of the astrocytes in the glutamate uptake [36]. In our study, the neuronal and the survival rate of the other cell types analyzed didn't decrease until they were exposed to very high concentrations of exogenous glutamate. Kritis et al described differences in the response to glutamate excitotoxicity by different cell lines, including oligodendroglial lineage cells, C6 rat glioma cells, primary cortical rat neurons, among others. They described that in some cell lines glutamate excitotoxicity is exerted through over activation of NMDA, AMPA, or kainate receptors whereas in other cell lines lacking such receptors, the toxicity is due to glutamate induced oxidative stress[37].

The in vitro measurements of glutamate after H-FIRE treatment did show statistical difference between treatments and controls, except for endothelial cells. After applying 250 V/cm H-FIRE treatment, the glutamate concentration was higher in astrocytes and neurons, and in F98 glioma cells we observed higher concentration in 1000 V/cm H-FIRE treatment group. However, the glutamate concentrations we observed are likely insufficient to produce cytotoxic or biological effects. We did not detect any effect of the H-FIRE treated cellular supernatants to increase the permeability of the endothelial monolayer. The effect of the glutamate in the permeabilization of the BBB es well described [12, 38-40], and is related to the activation of NMDA glutamate receptors, leading to produce calcium influx and nitric oxide (NO) synthesis. The NO can diffuse into the adjacent endothelial cells resulting in the increase of intracellular cGMP and consequent signaling cascade to produce changes in the conformation of the tight-junction proteins in the BBB [38]. We have demonstrated the effect of the H-FIRE treatment in the BBB opening in vivo, and this phenomenon is also mediated by tight-junction protein degradation and cytoskeletal changes, and our results suggest that the change in the endothelial permeability may not be dependent or related to the glutamate concentration [18].

Our results of in vivo experiments and in vitro experiments had some discordances, especially related to the glutamate concentration post- H-FIRE treatments. There were some limitations that make these results difficult to compare. In the in vivo study, we measured the glutamate with HPLC, and included a pooled sample of the brain tissue, and not specifically the glutamate release from each cell type. In the in vitro experiments,

because we were unable to generate adequate co-culture conditions of the different cell types, we couldn't more a representative environment of the brain tissue. We expected to have a higher concentration of glutamate in coculture conditions after H-FIRE treatment because of the role of F98 glioma cells in the brain microenvironment, their natural tolerance to excessive glutamate and the release by neurons vesicles. However, we would have observed the glutamate exposed cell survival, it was useful to determine the concentration in which we expected to have excitotoxicity occurring.

CONCLUSIONS

The results in in vivo studies showed that H-FIRE treatments increases glutamate concentrations, with quantitatively more glutamate released after applying ablation pulse protocol. The glutamate measured in F98 glioma implanted rats were significantly higher compared to healthy rat control. Also, the NMDA receptors and EAAT are upregulated in the 96 hours post-treatment group, as a response to the high glutamate in the brain tissue. However, the glutamate levels return to the basal concentration between 4-10 days post-treatment, likely related to the recovery of the BBB structure and the regulatory role of astrocytes and endothelial cells in the reuptake of glutamate. Our in vitro experiments indicated that while glutamate release occurs after H-FIRE treatment, the magnitude of the glutamate increase is likely not sufficient to produce significant cytotoxicity or increase BBB permeability, although this may reflect limitations of the in vitro model systems used.

REFERENCES

1. Hawkins, R.A., *The blood-brain barrier and glutamate.* Am J Clin Nutr, 2009. **90**(3): p. 867S-874S.
2. Hawkins, R.A. and J.R. Vina, *How Glutamate Is Managed by the Blood-Brain Barrier.* Biology (Basel), 2016. **5**(4).
3. Andras, I.E., et al., *The NMDA and AMPA/KA receptors are involved in glutamate-induced alterations of occludin expression and phosphorylation in brain endothelial cells.* J Cereb Blood Flow Metab, 2007. **27**(8): p. 1431-43.
4. Marcus, H.J., et al., *In vivo assessment of high-grade glioma biochemistry using microdialysis: a study of energy-related molecules, growth factors and cytokines.* J Neurooncol, 2010. **97**(1): p. 11-23.
5. Roslin, M., et al., *Baseline levels of glucose metabolites, glutamate and glycerol in malignant glioma assessed by stereotactic microdialysis.* J Neurooncol, 2003. **61**(2): p. 151-60.
6. Takano, T., et al., *Glutamate release promotes growth of malignant gliomas.* Nature Medicine, 2001. **7**(9): p. 1010-1015.
7. Lyons, S.A., et al., *Autocrine glutamate signaling promotes glioma cell invasion.* Cancer Res, 2007. **67**(19): p. 9463-71.
8. Noch, E. and K. Khalili, *Molecular mechanisms of necrosis in glioblastoma: the role of glutamate excitotoxicity.* Cancer Biol Ther, 2009. **8**(19): p. 1791-7.
9. Cederberg, H.H., N.C. Uhd, and B. Brodin, *Glutamate efflux at the blood-brain barrier: cellular mechanisms and potential clinical relevance.* Arch Med Res, 2014. **45**(8): p. 639-45.
10. Helms, H.C.C., et al., *Glutamate Transporters in the Blood-Brain Barrier.* Adv Neurobiol, 2017. **16**: p. 297-314.
11. Smith, Q.R., *Transport of glutamate and other amino acids at the blood-brain barrier.* J Nutr, 2000. **130**(4S Suppl): p. 1016s-22s.
12. Xhima, K., D. Weber-Adrian, and J. Silburt, *Glutamate Induces Blood-Brain Barrier Permeability through Activation of N-Methyl-D-Aspartate Receptors.* J Neurosci, 2016. **36**(49): p. 12296-12298.
13. De Bock, M., et al., *Endothelial calcium dynamics, connexin channels and blood-brain barrier function.* Prog Neurobiol, 2013. **108**: p. 1-20.
14. Arena, C.B., Sano, M.B., Rossmeisl, J.H., Caldwell, J.L., Garcia, P.A., Rylander, M.N., Davalos, R.V., *High- frequency irreversible electroporation (H-FIRE) for non-thermal ablation without muscle contraction.* Biomedical engineering online, 2011. **10**(1): p. 102.
15. Bhonsle, S.P., et al., *Mitigation of impedance changes due to electroporation therapy using bursts of high-frequency bipolar pulses.* Biomedical engineering online, 2015. **14**(Suppl 3): p. S3.
16. Ivey, J.W., et al., *Targeted cellular ablation based on the morphology of malignant cells.* Sci Rep, 2015. **5**: p. 17157.
17. Latouche, E.L., et al., *High-Frequency Irreversible Electroporation for Intracranial Meningioma: A Feasibility Study in a Spontaneous Canine Tumor Model.* Technol Cancer Res Treat, 2018. **17**: p. 1533033818785285.
18. Partridge, B.R., et al., *High-Frequency Irreversible Electroporation (H-FIRE) Induced Blood-Brain Barrier Disruption Is Mediated by Cytoskeletal Remodeling*

and Changes in Tight Junction Protein Regulation. Biomedicines, 2022. **10**(6).
19. Arena, C.B., et al., *Focal blood-brain-barrier disruption with high-frequency pulsed electric fields.* Technology, 2014. **02**(03): p. 206-213.
20. Lorenzo, M.F., et al., *Temporal Characterization of Blood-Brain Barrier Disruption with High-Frequency Electroporation.* Cancers (Basel), 2019. **11**(12).
21. Salford, L.G., et al., *A new brain tumor therapy combining bleomycin with in vivo electropermeabilization.* Biochemical and biophysical research communications, 1993. **194**(2): p. 938-943.
22. Agerholm-Larsen, B., et al., *Preclinical validation of electrochemotherapy as an effective treatment for brain tumors.* Cancer Res., 2011. **71**(11): p. 3753-62. Epub 2011 Apr 20.
23. Clarke, G., et al., *An isocratic high performance liquid chromatography method for the determination of GABA and glutamate in discrete regions of the rodent brain.* J Neurosci Methods, 2007. **160**(2): p. 223-30.
24. Rowley, H.L., K.F. Martin, and C.A. Marsden, *Determination of in vivo amino acid neurotransmitters by high-performance liquid chromatography with o-phthalaldehyde-sulphite derivatisation.* J Neurosci Methods, 1995. **57**(1): p. 93-9.
25. Lal, B.K., et al., *VEGF increases permeability of the endothelial cell monolayer by activation of PKB/akt, endothelial nitric-oxide synthase, and MAP kinase pathways.* Microvasc Res, 2001. **62**(3): p. 252-62.
26. Wang, W., W.L. Dentler, and R.T. Borchardt, *VEGF increases BMEC monolayer permeability by affecting occludin expression and tight junction assembly.* Am J Physiol Heart Circ Physiol, 2001. **280**(1): p. H434-40.
27. Zieminska, E., et al., *Glutamate, Glutamine and GABA Levels in Rat Brain Measured Using MRS, HPLC and NMR Methods in Study of Two Models of Autism.* Front Mol Neurosci, 2018. **11**: p. 418.
28. Lewerenz, J. and P. Maher, *Chronic Glutamate Toxicity in Neurodegenerative Diseases-What is the Evidence?* Front Neurosci, 2015. **9**: p. 469.
29. Dong, X.X., Y. Wang, and Z.H. Qin, *Molecular mechanisms of excitotoxicity and their relevance to pathogenesis of neurodegenerative diseases.* Acta Pharmacol Sin, 2009. **30**(4): p. 379-87.
30. Lai, T.W., S. Zhang, and Y.T. Wang, *Excitotoxicity and stroke: identifying novel targets for neuroprotection.* Prog Neurobiol, 2014. **115**: p. 157-88.
31. Schurr, A., et al., *Hypoxia, excitotoxicity, and neuroprotection in the hippocampal slice preparation.* J Neurosci Methods, 1995. **59**(1): p. 129-38.
32. Coulter, D.A. and T. Eid, *Astrocytic regulation of glutamate homeostasis in epilepsy.* Glia, 2012. **60**(8): p. 1215-26.
33. Ye, Z.C. and H. Sontheimer, *Glioma cells release excitotoxic concentrations of glutamate.* Cancer Res, 1999. **59**(17): p. 4383-91.
34. Kutzing, M.K., V. Luo, and B.L. Firestein, *Measurement of Synchronous Activity by Microelectrode Arrays Uncovers Differential Effects of Sublethal and Lethal Glutamate Concentrations on Cortical Neurons.* Annals of Biomedical Engineering, 2011. **39**(8): p. 2252-2262.
35. Zhang, Y. and B.R. Bhavnani, *Glutamate-induced apoptosis in neuronal cells is mediated via caspase-dependent and independent mechanisms involving calpain and caspase-3 proteases as well as apoptosis inducing factor (AIF) and this process*

is inhibited by equine estrogens. BMC Neurosci, 2006. **7**: p. 49.
36. Zhang, L.N., et al., *Astrocytes enhance the tolerance of rat cortical neurons to glutamate excitotoxicity.* Mol Med Rep, 2019. **19**(3): p. 1521-1528.
37. Kritis, A.A., et al., *Researching glutamate - induced cytotoxicity in different cell lines: a comparative/collective analysis/study.* Front Cell Neurosci, 2015. **9**: p. 91.
38. Vazana, U., et al., *Glutamate-Mediated Blood-Brain Barrier Opening: Implications for Neuroprotection and Drug Delivery.* J Neurosci, 2016. **36**(29): p. 7727-39.
39. Mayhan, W.G. and S.P. Didion, *Glutamate-Induced Disruption of the Blood-Brain Barrier in Rats.* Stroke, 1996. **27**(5): p. 965-970.
40. Collard, C.D., et al., *Neutrophil-derived Glutamate Regulates Vascular Endothelial Barrier Function*.* Journal of Biological Chemistry, 2002. **277**(17): p. 14801-14811.

CHAPTER 5. EFFECT OF THE HIGH FREQUENCY IRREVERSIBLE ELECTROPORATION ABLATION TREATMENT ON GLUTAMATE METABOLISM MEASURED BY H^1 MAGNETIC RESONANCE SPECTROSCOPY AND SPATIAL TRANSCRIPTOMICS IN DOGS WITH BRAIN TUMORS.

INTRODUCTION

One of the common clinical signs presents in canine patients with brain tumors is the seizures. Excitotoxicity is considered a main mechanism of epileptogenesis, as seizures are propagated primarily through excitatory glutamatergic transmission [1]. It is known that glutamate-induced excitotoxicity causes the neuronal death in epilepsy and increased glutamate levels were observed in epileptic human brain tissues and also in animal models of epilepsy [2]. Increased glutamate levels have been implicated in numerous seizure disorders, and glutamate can reach neurotoxic levels immediately preceding and during spontaneous seizures.

Glutamate has a close relationship with gliomas. Glioma cells release glutamate which causes excitotoxic death to surrounding neurons, thereby vacating room for tumor expansion [3]. Glutamate release occurs via system Xc, a cystine-glutamate exchanger that releases glutamate in exchange for cystine being imported for the synthesis of the cellular antioxidant GSH [4, 5]. It protects tumor cells from endogenously produced reactive oxygen and nitrogen species but also endows tumors with an enhanced resistance to radiation- and chemotherapy. Recent studies performed by our lab (data not published) showed an increase in the glutamate concentration after high frequency electroporation treatments in rodent model, more significantly in glioma cells implanted rat model compared to healthy control animals.

Recent studies have shown that proton magnetic resonance spectroscopy (1HMRS) can substantially improve the non-invasive categorization of human brain tumors, especially

for gliomas. It provides a non-invasive ‘window’ on biochemical processes within the brain [6], obtaining functional information in addition to anatomical information. Differentiation between low-grade and high-grade gliomas is important for estimating the prognosis and for therapeutic planning. Gliomas are heterogeneous and their spectra vary depending on the region sampled by 1HMRS. Therefore, multivoxel spectroscopy is generally considered preferable because it allows metabolic heterogeneity to be evaluated in different components of the tumor [7].

Differentiation between recurrent brain tumor and radiation change/injury is an important concern in postradiotherapy patients with brain tumors. 1HMRS is particularly helpful to distinguish radiation injury from tumor recurrence after radiotherapy. Decreased in Cho, NAA, and Cr are usually observed with radiation injury and high Cho/NAA ratio is suggestive of tumor recurrence [8].

Metabolites that are frequently interrogated with 1HMRS include alanine, aspartate, glucose, creatine, phosphocreatine, glutamine, glutamate, glycerophosphocholine, phosphocholine, lactate, lipids, myoinositol, N-acetyl aspartate (NAA), N-acetylaspartylglutamate, scylloinositol, glutathione, and taurine [9], and some of them are closely related to gliomas. NAA is a marker for neuronal density and viability and therefore is decreased in all diseases in which there is death of the neurons or replacement of neurons by other cells. The choline (Cho) contains contributions from glycerophosphocholine, phosphocholine and phosphatidylcholine. It reflects the metabolism of cellular membrane turnover and therefore is increased in all processes leading to hypercellularity [7]. Creatine (Cre) had contributions from creatine phosphate, gamma-aminobutyric acid, lysine and glutathione and serves as a marker for energy-dependent systems in the brain cells [10]. Glx complex (Glx) is the group composed by glutamate and glutamine [11], and is detected in brain tumor patients, and a rise of Glx peak may relate to a role of glutamate as an excitotoxin in accelerated cell proliferation of malignant brain tumors [10]. Also, lactate is another metabolite and indicates the presence of anerobic or nonoxidative metabolism, e.g. in abscess or necrosis. Myo-inositol (Myo) It is considered as a glial marker because it is primarily synthesized in glial cells, almost only in astrocytes and participates in their

osmoregulatory system [7]. Myo is also involved in the activation of protein C kinase. Protein C kinase leads to production of proteolytic enzymes, which are found more often in malignant and aggressive primary cerebral tumors [12].

Another informative method to study the metabolism of glutamate in gliomas is spatial transcriptomics. It is an emerging class of high-throughput technologies that enable biologists to systematically investigate the expression of genes along with spatial information. With spatially resolved transcriptomic methods, scientists can get transcriptomic data and know the positional context of those cells in a tissue. Brain tumors, in particular, are complex cellular environments, and single-cell RNA-seq has been used to show how multiple parallel tumor clones are intermingled with normal neurons and glia as well as activated immune and vascular cells [13]. To fully understand the interplay of cell-cell interactions and complex differentiation in tumors, spatial transcriptomics will be an invaluable contribution.

GeoMx is a digital spatial profiling instrument produced by NanoString and it differentiate itself by its ability to work on notoriously difficult formalin fixed paraffin embedded samples. It works in an iterative manner, where the user manually selects regions of interest (ROIs) via microscopy of varying sizes (10–600 μm in diameter). These regions are then excited with UV light, triggering the release of either RNA target probe (mRNA assay) or antibody (protein assay) coupled barcoded tags. In the current commercial form, the tags are collected and quantified with the NanoString nCounter instrument, putting a limit to multiplex capacity.

The objective of this study is to characterize the effect of the H-FIRE treatment in the glutamate metabolism in canine patients with naturally occurring brain tumors, using 1HMRS and GeoMx digital spatial profiling. ***Our central hypothesis is that H-FIRE will increase the glutamate concentration after treatment because of the cell membrane permeating mechanism and ablation effects of H-FIRE, and glutamate related gene expression in the tumor center will be up-regulated compared to the tumor periphery.***

MATERIAL AND METHODS

Animals: we used a total of 8 dogs from the Veterinary Teaching Hospital of Virginia-Maryland College of Veterinary Medicine. We included 3 canine patients with histologically diagnosed intracranial meningiomas, 2 with oligodendrogliomas and 3 healthy controls for the study (IACUC protocols 16-107 and 18-048 [14]).

H-FIRE Treatment: The H-FIRE treatment protocols utilized in these dogs was described previously by LaTouche 2018 [14].

H1 Magnetic Resonance Spectroscopy (1HMRS): While under general anesthesia, and prior to administration of HFIRE treatment, an MRI examination of the brain performed using standard morphologic sequences as well as multivoxel H^1 MRS sequence using a 1.5T superconducting magnet (Philips Intera, Andover, MA, USA) as previously described [15]. Then, the HFIRE treatments were administered as described previously [14]. One hour after completion of the HFIRE treatment, another multivoxel H^1 MRS sequence was obtained. Following completion of imaging, the multi-voxel spectroscopy acquisitions (ROI) were post-processed, and three smaller ($5mm^3$) spherical regions of interest (ROI) from the larger, rectangular multi-voxel spectroscopy acquisition grid was obtained (Figure 5-1) from pre- and post-treatment scans. These ROI were placed in consistent locations within the original (larger) multivoxel spectroscopy region of tissue interrogation (Figure 5-1) such that one ROI is placed within the central tumor mass in the ablated region, one ROI is placed at the periphery of the tumor in the region of BBB HFIRE induced BBB disruption, and the final ROI will be placed in normal appearing brain tissue in the contralateral hemisphere of the brain.

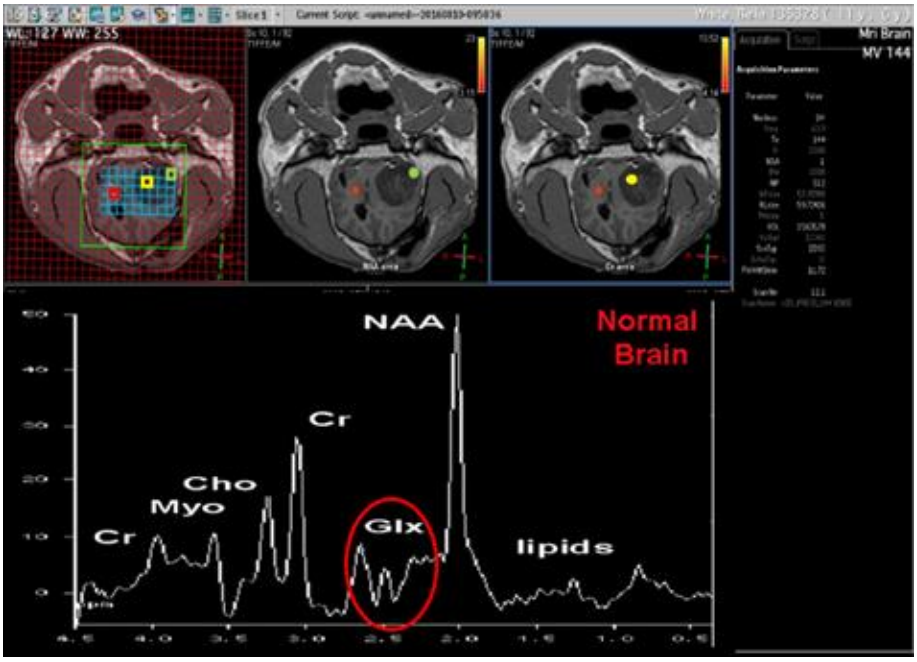

Figure 5-1. Multivoxel H1 MRS in a dog with malignant glioma with ROI in the contralateral normal brain (red), center of tumor mass targeted for ablation with HFIRE (yellow) and peripheral region of expected BBB disruption (green) to be interrogated for glutamate (Glx; red) concentrations. The spectra provided is from a normal brain region.

We analyzed a total of 5 metabolites: NAA, Glx complex, Choline, Creatine and Myoinositol. Relative metabolite concentrations from each of the ROI was measured by using the automated data processing spectral fitting linear combination model alogorithm program (LCModel). LCModel analysis method is particularly attractive for the evaluation of uncertainty (i.e., Cramer-Rao lower bounds). This program automatically adjusts the phase and chemical shift of the spectra, estimated the baseline, and performs eddy current correction. Relative metabolite peak areas and their uncertainties were estimated by fitting the spectrum to a standard set of spectra acquired from known solutions of metabolites. The software program quantifies metabolite peak areas by reference to the peak for the water-unsuppressed image. Briefly, peak signals of metabolites from the water-suppressed spectrum will be divided by those from a water-unsuppressed spectrum, while applying corrections (differences in T1 and T2 relaxation times between the metabolite and water and the number of 1H nuclei contributing to the metabolite and water peaks). This result in a molal concentration of the metabolite, and quantitative results were reported as error

estimates, which are the Cramer-Rao lower bounds. The metabolite peak areas measured by use of the 1H MRS data between the 2 groups and ROI (pre- and post-HFIRE treatments) were compared by use of a Mann-Whitney U test. A nonparametric test was chosen because of the small sample size.

Spatial Transcriptomic Profiling of Canine Tumor Biopsies: We used spatial profiling technology based on a human whole transcriptomic atlas (WTA; GeoMx Digital Spatial Profiler [DSP], Nanostring, Seattle, WA) to compare geographic regions canine tumor biopsies pre- and post- HFIRE treatment**.** The WTA consists of 18,000+ gene probes involved in neural signaling, neuroinflammation, and brain cancer, of which 14,500 genes share > 85% identity with the dog, as measured using % identity with BLASTn (https://blast.ncbi.nlm.nih.gov/) to estimate cross-reactivity within species.

The DSP uses a patented DNA barcoding technology in which synthetic DNA oligonucleotide barcodes are attached to in situ probes for mRNA detection via a UV photocleavable linker. The GeoMx DSP portfolio provides pre-validated content in both oncology and neuroscience. All RNA probes go through a robust validation pipeline so you can use the reagents off the shelf. A single tissue section is labeled with a cocktail of these probes and fluorescently labeled morphology markers. The fluorescent morphology markers, in our case pancytokeratin and nuclear (DAPI) stains, were done using well established manual methods [16]. Regions of interest (ROI) for molecular profiling are selected by the end user based on the fluorescent images using the DSP software interface (Figure 5-2), and UV light illuminates each region independently, which releases the barcodes from that region for subsequent counting. As barcodes are released, a microcapillary system sips up the tags, and dispenses them into a 96 well microtiter plate. Those barcodes can then be read out on an Illumina sequencer. Molecular counts for each target in the panel can then be mapped back to distinct ROI and comparisons made within and between samples.

We comparatively analyzed 4 ROI placed on 2 geographic regions (n=2 ROI/region) from each dog's pre- and post-tumor samples that include: 1) untreated bulk tumor in the region

of gadolinium enhancement, and 2) transition zone between treated necrotic (or naturally necrotic area) (Figure 5-2). The third region (necrotic tumor) data had several ROI that did not pass quality control, so those were excluded from analyses. Assay quality control was determined using sequencing saturation and Q3 normalization methods, which uses the top 25% of expressers to normalize across ROIs, so it is robust to changes in expression of individual genes and ideal for making comparisons across ROIs [17]. We focused our analyses on 400 genes involved in glutamate receptor signaling, glutamate transporters, and glutamate metabolism.

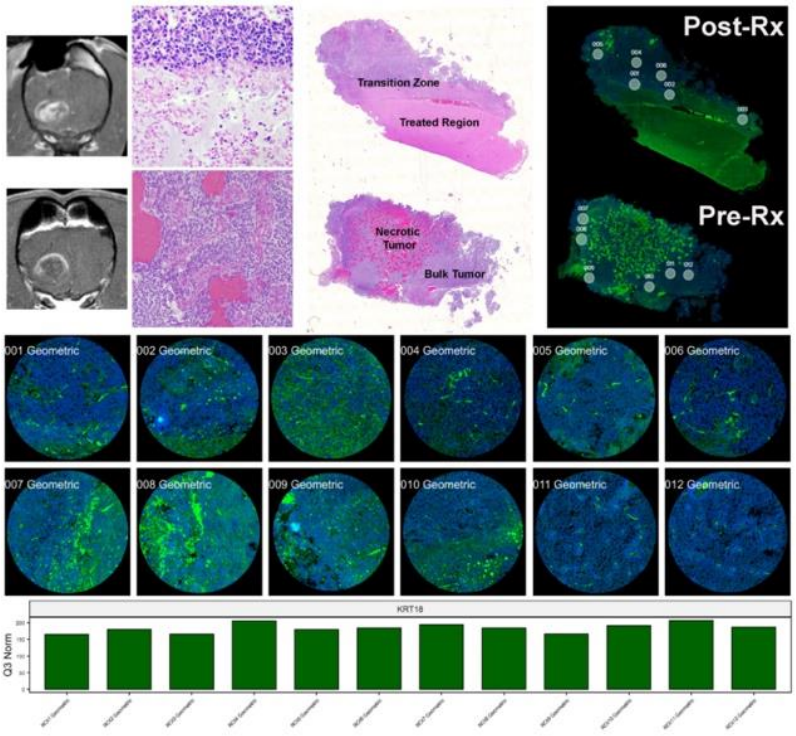

Figure 5-2. GeoMx DSP spatial transcriptomic analytic ROI selection software interface comparing canine glioma biopsies pre- and post-HFIRE treatment. Up to 12 ROI may be placed on a single slide for analysis, and in this case 6 ROI are selected from 3 geographic of each tumor pre- and post-treatment.

Data analyses were performed in the Rosalind bioinformatics software environment (https://www.rosalind.bio/bioinformatics), and for the purposes of this experiment we limited data analysis to 400 genes involved in glutamatergic metabolism. To visualize large-scale variability between samples, we used dimensional reduction principal component analysis (PCA) to assess similarities between genes and groups when a large

number of variables are measured. Differential gene expression between groups (ie treatment and ROI) will be examined using volcano plots. We used gene set enrichment analysis (GSEA) to determine whether a priori defined set of genes show statistically significant, concordant differences between ROI in pre- and post-treatment biological phenotypes. We also leveraged GSEA to calculate normalized enrichment scores (NES), identifying pathways significantly differently expressed up or down in the context of the pre- and post HFIRE treatment states. Pathway changes were further visualized using the GO-KEGG pathway database.

RESULTS

H1 Magnetic Resonance Spectroscopy (1HMRS)

The values of the metabolite measurements pre- and post- H-FIRE treatment are summarized in the Figure 5-3.

We observed a significant decrease in the levels of NAA (Figure 5-3A), Creatine (Figure 5-3C) and Myoinositol (Figure 5-3E) in the brain tumor ROI compared to the healthy brain tissue ROI, in both meningioma and oligodendroglioma samples. Statistical differences were observed between the pre- and post- treatment measurements in NAA and Myoinositol of oligodendroglioma samples, where NAA was decreased post-treatment both in tumor core and periphery, meanwhile Myoinositol was decreased post-treatment only in the tumor center.

Choline values were statistically higher in the brain tumor ROIs compared to the healthy brain tissue ROIs (Figure 5-3B). No statistical differences were observed between the pre- and post- treatment measurements.

For the Glx complex, the measurements in oligodendroglioma patients were significantly higher compared to the control and meningioma patients. The tumor center had higher Glx complex values compared to the tumor periphery, and post-treatment measurement was

significantly higher compared to the pre-treatment measurements in both tumor core and periphery (Figure 5-3D).

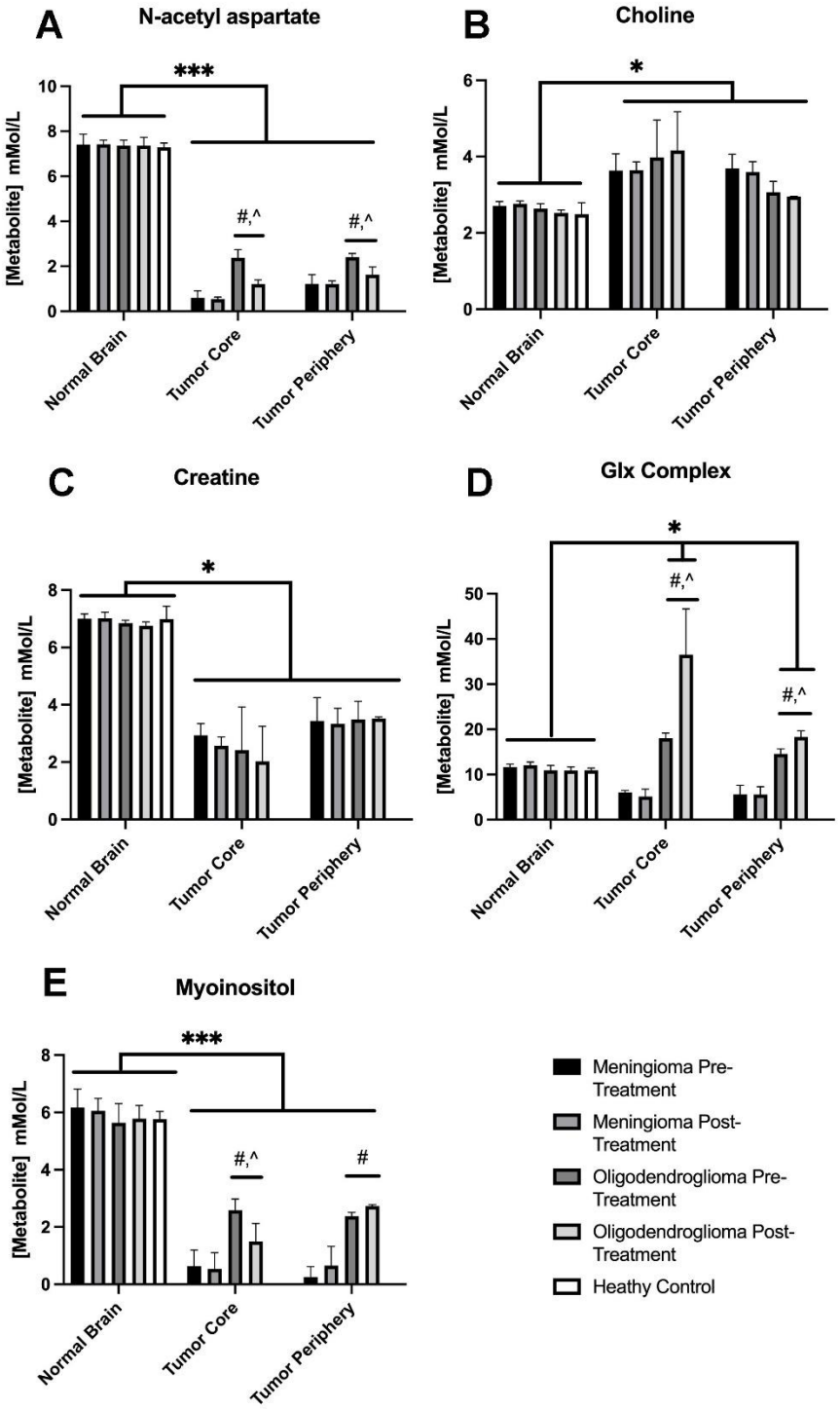

Figure 5-3. 1HMRS metabolite measurements in normal brain, tumor center and tumor periphery. An asterisk (*) indicates that the labeled measurements significantly ($p<0.05$) different from normal brain ROI. The (***) indicates $p<0.001$. The (#) indicates that measured analyte significantly different ($p<0.05$) between tumor types (meningioma vs. oligodendroglioma) in the given ROI. The (^) indicates that pre-and post-treatment values for the measured analyte significantly different ($p<0.05$) for that tumor type in that ROI.

Spatial Transcriptomics

We analyzed genes related directly to glutamate metabolism, and we compared them pre- and post- H-FIRE treatment in the tumor center and the tumor periphery area. For AMPA receptor genes (GRIA1, GRIA2, GRIA3, GRIA4), post-treatment we found that they are significantly downregulated in the tumor area and upregulated in the tumor periphery (Figure 5-4). Kainate receptor genes (GRIK2), were downregulated post-treatment in both tumor center and periphery (Figure 5-5).

The NMDA receptor gene (GRIN3A), was upregulated post-treatment in both the tumor center and periphery (Figure 5-6). Metabotropic glutamate receptor genes (GRM2, GRM6), specifically in the tumor center, were upregulated post-treatment (Figure 5-7). The EAAT receptor gene, Slc1A4, was upregulated and Slc1A6 was downregulated in the tumor periphery area post-treatment (Figure 5-8). No differences in EAAT genes were observed in the tumor center. The calcium signaling pathway gene PPP2CB were significantly upregulated post-treatment in both tumor center and periphery areas (Figure 5-9).

The components of the glutamatergic signaling pathway represented by the significantly up- or downregulated genes of the tumor core and tumor periphery comparing pre- and post-H-FIRE treatment in our dataset are summarized in Figure 5-10 and Figure 5-11.

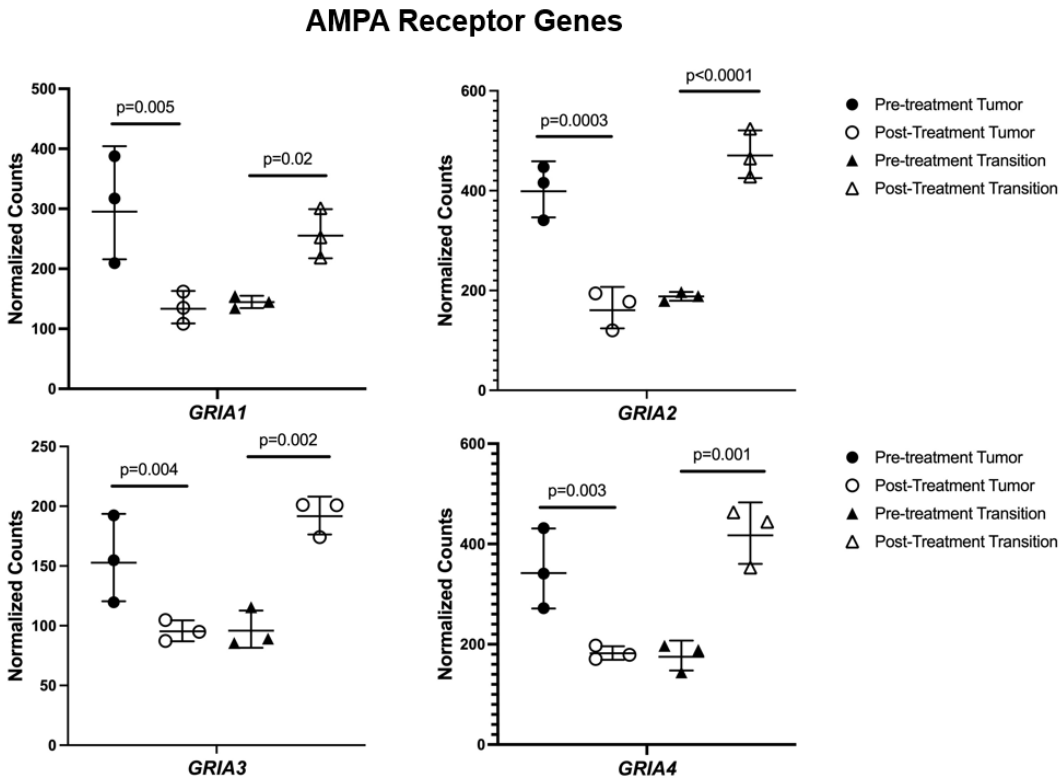

Figure 5-4. AMPA receptor gene expression in tumor center and tumor periphery

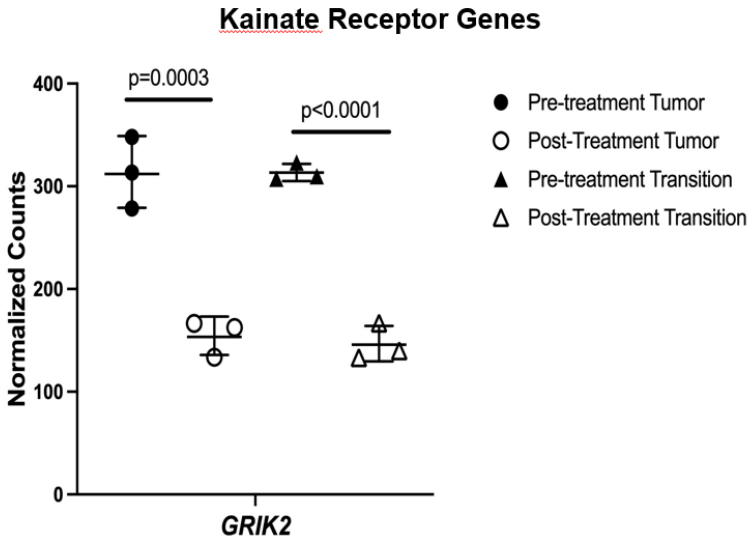

Figure 5-5. Kainate receptor gene expression in tumor center and tumor periphery

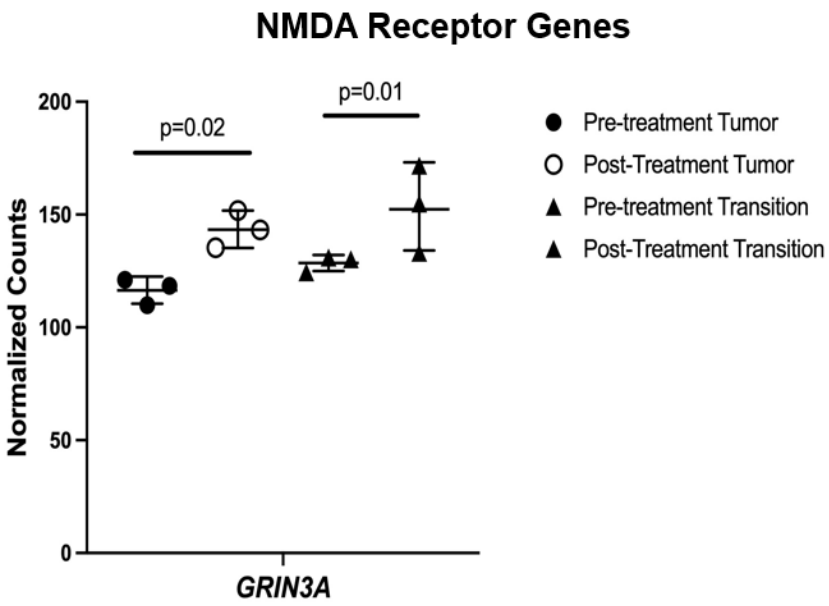

Figure 5-6. NMDA receptor gene expression in tumor center and tumor periphery

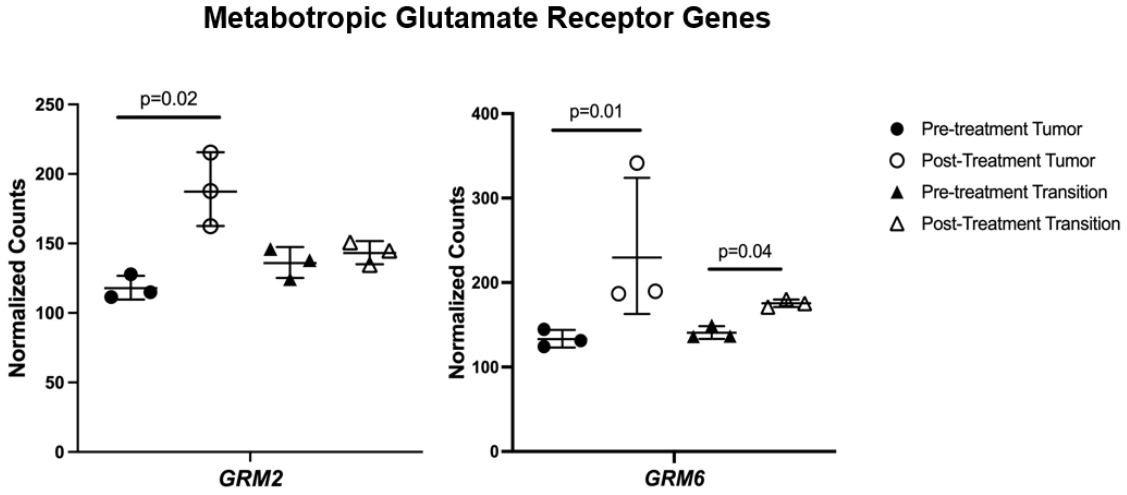

Figure 5-7. Metabotropic Glutamate receptor gene expression in tumor center and tumor periphery

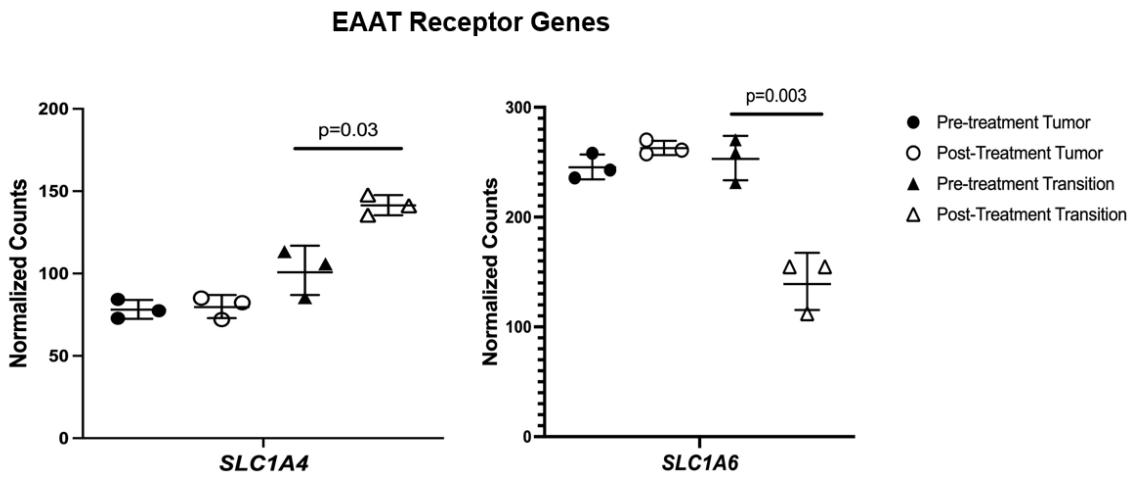

Figure 5-8. EAAT receptor gene expression in tumor center and tumor periphery

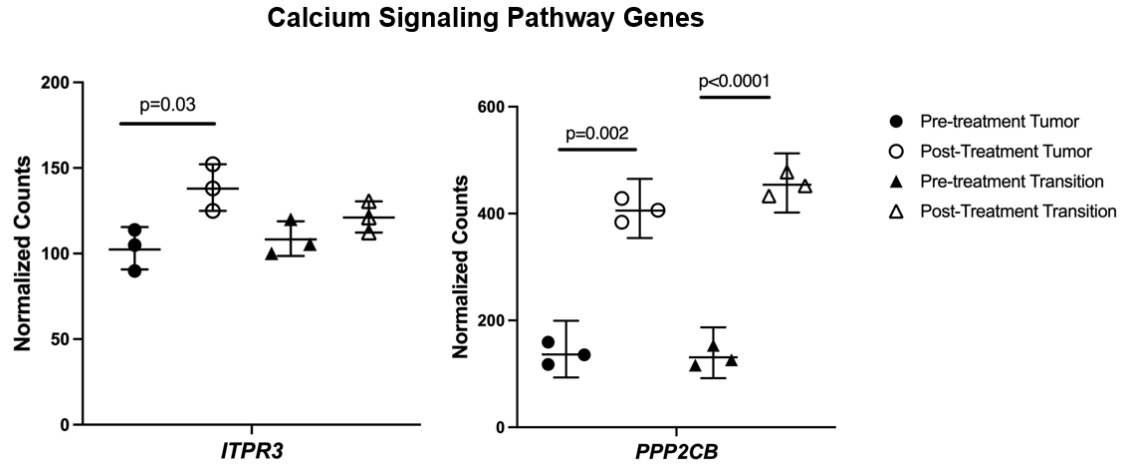

Figure 5-9. Calcium signaling pathway gene expression in tumor center and tumor periphery

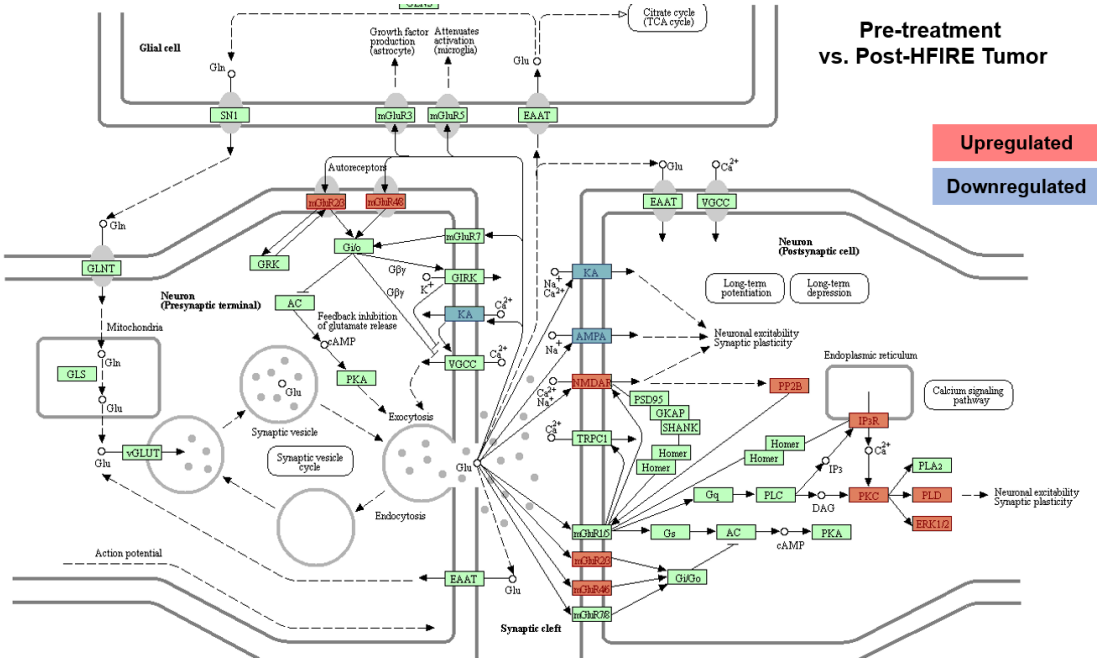

Figure 5-10. Components of the glutamatergic signaling pathway upregulated (red) and downregulated (blue) in the tumor core compared pre- and post- H-FIRE treatment

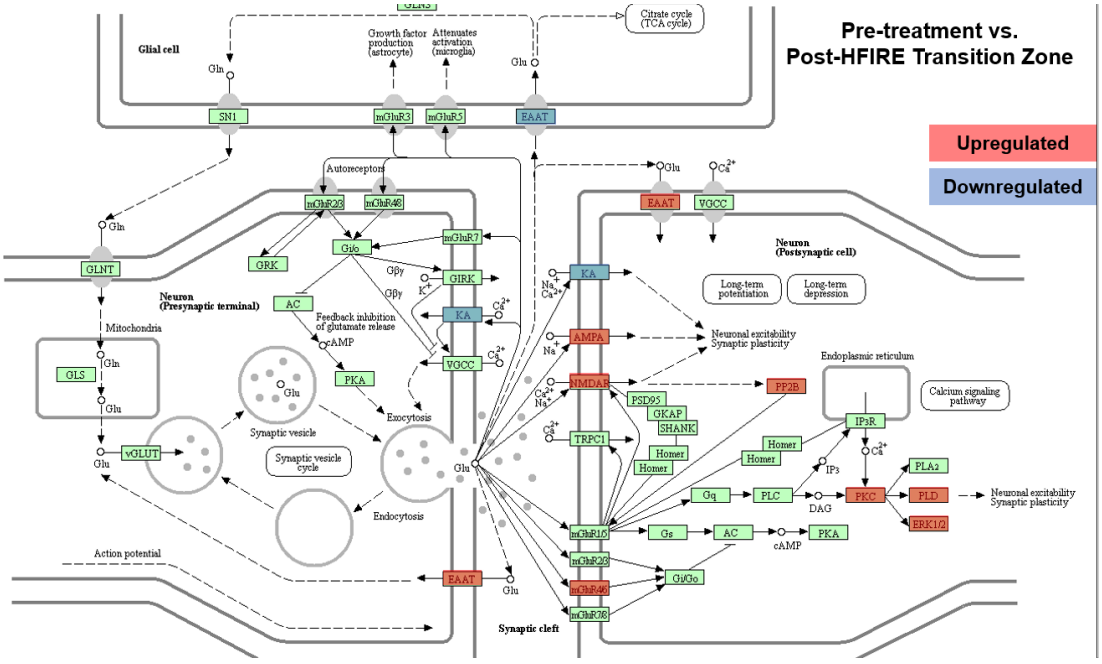

Figure 5-11. Components of the glutamatergic signaling pathways upregulated (red) and downregulated (blue) in the tumor periphery compared pre- and post- H-FIRE treatment

DISCUSSION

Our 1HMRS results are concordant with the human literature with what is expected for the measured metabolites in untreated brain tumors: decreased NAA and Cre, increased Cho and Glx complex [7]. Our finding of a significantly lower levels of myoinositol in canine meningioma and oligodendroglioma patients, with the highest values in the control group, was unexpected. It is anticipated that myoinositol should be lower in meningioma patients, but we expected to have higher values in oligodendroglioma dogs compared to healthy brain. One of the possibly explanations for this result is that the ROI placement was not totally in tumor tissue and it included necrotic area or the heterogeneous cystic area of the tumor.

The decrease in NAA is widely interpreted as the loss, dysfunction or displacement of normal neuronal tissue since NAA is believed to be primarily of neuronal and axonal origin. The Cho signal are involved in membrane synthesis and degradation; it has been suggested that it is increased in brain tumors due to increased membrane turnover. Cho has also been found to correlate well with the cellular density of the tumor. Increased levels of Myo in oligodendroglioma were, as these tumors contain increased numbers of glial cells, which have been reported to contain high levels of myoinositol, and in particular have been reported to be high in grade II gliomas [10].

Regarding the Glx complex, it is also well described the relationship between glutamate and gliomas and how glioma cells contribute to increase the glutamate concentration in the extracellular fluid [18]. Our results also reflect the higher levels of the Glx complex, and more interestingly, there is a significantly increase in the tumor center ROI after the H-FIRE treatment was performed. The concentration of Glx complex post-treatment in the tumor core was 36.51 mMol/L, a concentration at which the excitotoxicity theoretically could occur. This result could be related to the cell permeation mechanism and the ablation and resultant death of the glioma cells that contributes to an acute increase of the glutamate levels, as histologic ablations were demonstrated in the dogs treated with HFIRE in our study. Clinically this is very important because it is well known the damage that causes the

excitotoxicity in the brain, reflected as seizures. We might anticipate the possible complication of the excitotoxicity induced seizures after H-FIRE treatment, as seizures were a complication of treatment observed in two of the dogs treated here. Using a glutamate receptor antagonist should be considered to mitigate the appearance of seizures.

One limitation of our data is that we obtained the post-treatment measurements 1 hour after the H-FIRE was performed. We know from our previous research describing the temporal characterization of H-FIRE induced BBBD [14, 19, 20] and the measurements of glutamate presented in Chapter 4 in rodent models that the glutamate concentrations increased over 24-72 hours post-treatment in healthy and glioma-bearing rat brains. Thus, our sampling window could have underestimated the peak post-treatment glutamate concentration in the dogs. It will be interesting to make serial measurements of Glx complex in dog patients using 1HMRS and describe how the glutamate concentration changes over the time.

With respect to the Glx complex in meningioma patients, Crisi [21] described the presence and the relevance of the Glx metabolic pattern in human meningioma patients, and they also didn't observe statistical differences between the meningioma and normal brain Glx concentration, which is also consistent with our results. Given that that meningiomas are composed of mesenchymal tumoral and stromal elements, and not neuroepithelial cells, this Glx pattern is not unexpected.

When comparing the glutamate metabolism and signaling in the pre- and post-treatment in the center of the tumor tissue, we observed that the NMDA receptor genes are upregulated. Activation of NMDA receptors can increase the vascular permeability in the BBB and was described by Vazana et al. [22]. Also, overstimulation of glutamate receptors causes the increased influx of Ca^{2+} and Na+ through ion channels, which is followed by the transport of Cl- and water. Postsynaptic neurons are overloaded by extracellular Ca^{2+} and Na+ as well as intracellular Ca^{2+} released from mitochondria. This combined Ca^{2+} overload leads to a metabolic damage in the cell resulting in necrosis [23, 24]. We also observed an upregulation of the calcium signaling pathway post-treatment in the tumor core and in the transition area, explaining possibly the role of calcium in the excitotoxicity mechanism

caused by the H-FIRE treatment, combined with the upregulation of the different glutamate receptor genes. As the mechanisms of H-FIRE induced cell death are still being elucidated, it is also plausible that the upregulated calcium signaling pathways we observed, some of which are known to be critical pro-apoptotic factors, which are were activated by another upstream signal besides glutamate release. Metabotropic glutamate receptor genes were also upregulated in the tumor bulk post-H-FIRE, and it could be explained as a response to the high increase of the Glx complex observed in the 1HMRS data.

Looking to the transition zone gene expression, we found a very similar result as the tumor center area. However, it was interesting to see the upregulation of EAAT gene in the neuronal membrane, but a downregulation in the glial cells membrane. Related to the high Glx complex observed in the 1HMRS data post-treatment, we expected to have the upregulation of EAAT genes to regulate the glutamate concentration in the extracellular fluid by the normal brain tissue in the transition zone. This could be due to a potential selectivity of HFIRE to preferentially kill malignant glial cells. Alternatively, we may case the downregulation of EAAT genes to the glioma cells through an upregulation of SXC and downregulation of EAAT [25, 26].

CONCLUSIONS

H-FIRE treatment in canine patients with brain tumors, specifically with oligodendrogliomas, increases the levels of Glx complex, and its principal component is the glutamate neurotransmitter. Analyzing the glutamate related gene expression of the oligodendroglioma in the biopsies using the GeoMx DSP we observe the upregulation of NMDA receptor genes and metabotropic glutamate receptor genes in the tumor center area, and additionally an upregulation of EAAT genes in the neuronal membrane in the transition area, possibly explained as a response to the high concentration of glutamate produced by the treatment effect. Additional investigations are warranted in order to determine the potential clinical or biologic significance of increased glutamate release following H-FIRE treatment.

REFERENCES

1. Chapman, A.G., *Glutamate and epilepsy.* J Nutr, 2000. **130**(4S Suppl): p. 1043s-5s.
2. Haglid, K.G., et al., *Excitotoxicity. Experimental correlates to human epilepsy.* Mol Neurobiol, 1994. **9**(1-3): p. 259-63.
3. Sontheimer, H., *A role for glutamate in growth and invasion of primary brain tumors.* J Neurochem, 2008. **105**(2): p. 287-95.
4. Buckingham, S.C., et al., *Glutamate release by primary brain tumors induces epileptic activity.* Nature Medicine, 2011. **17**(10): p. 1269-1274.
5. Natarajan, S.K. and S. Venneti, *Glutamine Metabolism in Brain Tumors.* Cancers (Basel), 2019. **11**(11).
6. Tognarelli, J.M., et al., *Magnetic Resonance Spectroscopy: Principles and Techniques: Lessons for Clinicians.* J Clin Exp Hepatol, 2015. **5**(4): p. 320-8.
7. Bulik, M., et al., *Potential of MR spectroscopy for assessment of glioma grading.* Clin Neurol Neurosurg, 2013. **115**(2): p. 146-53.
8. Elias, A.E., et al., *MR spectroscopy using normalized and non-normalized metabolite ratios for differentiating recurrent brain tumor from radiation injury.* Acad Radiol, 2011. **18**(9): p. 1101-8.
9. Alger, J.R., *Magnetic Resonance Spectroscopy*, in *Encyclopedia of Neuroscience*, L.R. Squire, Editor. 2009, Academic Press: Oxford. p. 601-607.
10. Horská, A. and P.B. Barker, *Imaging of brain tumors: MR spectroscopy and metabolic imaging.* Neuroimaging Clin N Am, 2010. **20**(3): p. 293-310.
11. Bertholdo, D., A. Watcharakorn, and M. Castillo, *Brain proton magnetic resonance spectroscopy: introduction and overview.* Neuroimaging Clin N Am, 2013. **23**(3): p. 359-80.
12. Castillo, M., J.K. Smith, and L. Kwock, *Correlation of myo-inositol levels and grading of cerebral astrocytomas.* AJNR Am J Neuroradiol, 2000. **21**(9): p. 1645-9.
13. Patel, A.P., et al., *Single-cell RNA-seq highlights intratumoral heterogeneity in primary glioblastoma.* Science, 2014. **344**(6190): p. 1396-401.
14. Latouche, E.L., et al., *High-Frequency Irreversible Electroporation for Intracranial Meningioma: A Feasibility Study in a Spontaneous Canine Tumor Model.* Technol Cancer Res Treat, 2018. **17**: p. 1533033818785285.
15. Ober, C.P., et al., *Optimizing a protocol for (1) H-magnetic resonance spectroscopy of the canine brain at 3T.* Vet Radiol Ultrasound, 2013. **54**(2): p. 149-58.
16. Lazarus, J., et al., *Optimization, Design and Avoiding Pitfalls in Manual Multiplex Fluorescent Immunohistochemistry.* J Vis Exp, 2019(149).
17. Li, X., et al., *Choice of library size normalization and statistical methods for differential gene expression analysis in balanced two-group comparisons for RNA-seq studies.* BMC Genomics, 2020. **21**(1): p. 75.
18. Lange, F., J. Hornschemeyer, and T. Kirschstein, *Glutamatergic Mechanisms in Glioblastoma and Tumor-Associated Epilepsy.* Cells, 2021. **10**(5).
19. Lorenzo, M.F., et al., *Temporal Characterization of Blood-Brain Barrier Disruption with High-Frequency Electroporation.* Cancers (Basel), 2019. **11**(12).
20. Ivey, J.W., et al., *Targeted cellular ablation based on the morphology of malignant cells.* Sci Rep, 2015. **5**: p. 17157.
21. Crisi, G., *(1)H MR Spectroscopy of Meningiomas at 3.0T: the Role of Glutamate-*

Glutamine Complex and Glutathione. Neuroradiol J, 2011. **24**(6): p. 846-53.
22. Vazana, U., et al., *Glutamate-Mediated Blood-Brain Barrier Opening: Implications for Neuroprotection and Drug Delivery.* J Neurosci, 2016. **36**(29): p. 7727-39.
23. Yalcin, G. and A. Yalcin, *Excitotoxicity as a molecular mechanism in Epilepsy.* Geriatric Medicine and Care, 2018. **2**(1).
24. Dong, X.X., Y. Wang, and Z.H. Qin, *Molecular mechanisms of excitotoxicity and their relevance to pathogenesis of neurodegenerative diseases.* Acta Pharmacol Sin, 2009. **30**(4): p. 379-87.
25. Ye, Z.C., J.D. Rothstein, and H. Sontheimer, *Compromised glutamate transport in human glioma cells: reduction-mislocalization of sodium-dependent glutamate transporters and enhanced activity of cystine-glutamate exchange.* J Neurosci, 1999. **19**(24): p. 10767-77.
26. Ye, Z.C. and H. Sontheimer, *Glioma cells release excitotoxic concentrations of glutamate.* Cancer Res, 1999. **59**(17): p. 4383-91.

CHAPTER 6. FUTURE DIRECTIONS

Brain tumors are a great challenge for both human and veterinary medicine. The technological advances of recent decades in the area of medicine have meant that brain tumor treatments are constantly evolving. Our laboratory plays an important role in translating comparative data between canine patients and human patients suffering from brain tumors. For this reason, our research has focused on the development of innovative techniques for diagnosis and treatment. Our collective work shows that the CETCS and H-FIRE are promising devices for the treatment brain tumors.

The safety evaluation of these techniques is an important part of anticipating possible complications and taking measures to avoid them. In this sense, the work presented provides us with important information when applying the different treatment alternatives, improving the effectiveness of out therapies and the health of our patients. Ongoing clinical trials for our dog patients with brain tumors will continue to give us valuable information that can be translated to human glioblastoma patients.

As the cellular mechanisms of how H-FIRE induces cell death are not fully known, the methods we used have more potential to contribute to our molecular understanding of H-FIRE. Further interrogating our spatial transcriptomic data will allow us to study multiple other genes and signaling pathways related to cell death, such as apoptosis, pyroptosis, or ferroptosis that may be involved in this complex process.

We have demonstrated in our work that there is a an increase in glutamate concentration after H-FIRE treatment was performed in vivo, but we do not know if this is clinically significant. Another approach to study the potential clinical significance of glutamate excitotoxicity would be to correlate the clinical signs and adverse events to the pre- and post-H-FIRE glutamate concentrations in larger cohort of dogs with brain tumors. Glutamate could be measured indirectly and directly by different in vivo measurement techniques, including 1HMRS, brain microdialysis, or HPLC from biopsies, and perform

comparisons between the methods to potentially identify the threshold of glutamate that may causes clinically detectable effect of excitotoxicity, principally reflected as seizures. This study could be further extended by pre-treating a subgroup of dogs with a glutamatergic antagonist, such as levetiracetam, to determine if this approach either reduces the post-treatment glutamate release and/or attenuates the development of complications.

Determining the exact mechanism of cell death or biological significance of glutamate release may lead to better combinatorial treatments, or interventions to mitigate against possible complications associated with treatment, measures which will ultimately improve the outcome of patients with this devastating disease.